Article

Cell Reports

PI3K-Mediated Blimp-1 Activation Controls B Cell Selection and Homeostasis

Graphical Abstract

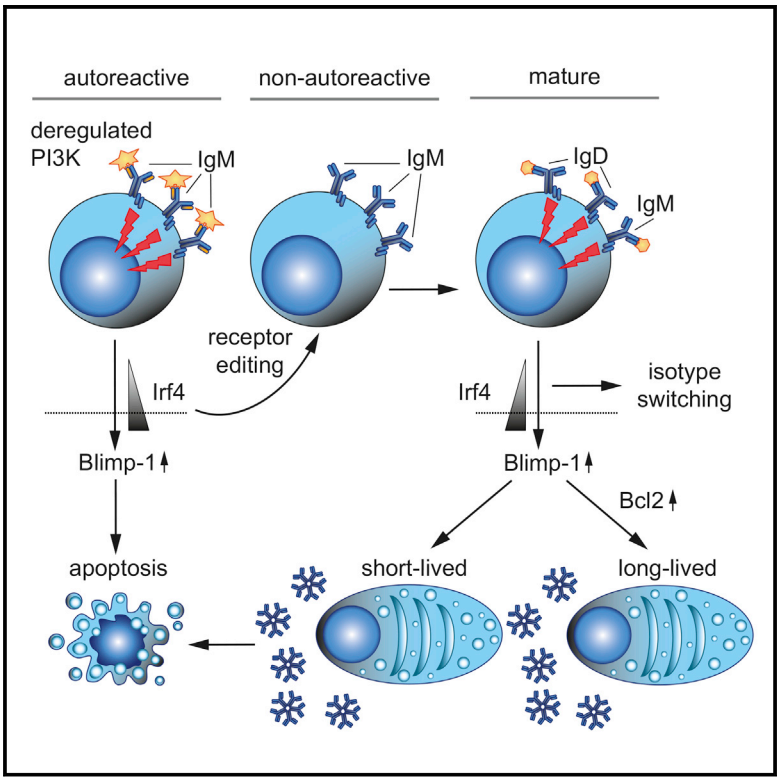

Authors

Corinna S. Setz, Eva Hug, Ahmad Khadour, Hend Abdelrasoul, Mayas Bilal, Elias Hobeika, Hassan Jumaa

Correspondence

hassan.jumaa@uni-ulm.de

In Brief

Setz et al. show that BCR-mediated activation of PI3K induces the terminal differentiation factor Blimp-1 that interferes with cell cycling and survival, thereby preventing the expansion of activated B cells. Thus, the interplay between PI3K activity and regulation of terminal differentiation determines proper selection and expansion of developing B cells.

Highlights

- B cell expansion is normal despite increased PI3K activity after Pten deletion
- Deregulated PI3K induces Blimp-1 and leads to premature terminal differentiation
- Premature terminal differentiation prevents expansion of activated B cells
- Expansion of B-1 B cells by autoreactive BCR and defective terminal differentiation

Setz et al., 2018, Cell Reports *24*, 391–405
July 10, 2018
https://doi.org/10.1016/j.celrep.2018.06.035

CellPress

Cell Reports
Article

PI3K-Mediated Blimp-1 Activation Controls B Cell Selection and Homeostasis

Corinna S. Setz,[1] Eva Hug,[1,3] Ahmad Khadour,[1] Hend Abdelrasoul,[1,2] Mayas Bilal,[1] Elias Hobeika,[1] and Hassan Jumaa[1,4,*]
[1]Institute of Immunology, University Medical Center Ulm, 89081 Ulm, Germany
[2]Genetic Engineering and Biotechnology Division, Molecular Biology Department, National Research Centre (NRC), 12622 Giza, Egypt
[3]Present address: MyeloProDiagnostics and Research GmbH, 1090 Vienna, Austria
[4]Lead Contact
*Correspondence: hassan.jumaa@uni-ulm.de
https://doi.org/10.1016/j.celrep.2018.06.035

SUMMARY

Activation of phosphoinositide 3-kinase (PI3K) signaling plays a central role in regulating proliferation and survival of B cells. Here, we tested the hypothesis that B cell receptor (BCR)-mediated activation of PI3K induces the terminal differentiation factor Blimp-1 that interferes with proliferation and survival, thereby controlling the expansion of activated B cells. In fact, B-cell-specific inactivation of Pten, the negative regulator of PI3K signaling, leads to deregulated PI3K activity and elevated Blimp-1 expression. Combined deficiency for Pten and Blimp-1 results in abnormal expansion of B-1 B cells and splenomegaly. Interestingly, Blimp-1 also acts at early stages of B cell development to regulate B cell selection, as Blimp-1 deficiency results in an increased proportion of autoreactive B cells. Together, our data suggest that the combined requirement of deregulated PI3K signaling in addition to defective terminal differentiation represents the basis for proper selection and expansion of developing B cells.

INTRODUCTION

Phosphoinositide 3-kinase (PI3K) is a central B cell receptor (BCR)-associated signaling axis that regulates diverse functions in developing B cells. Following BCR engagement (Depoil et al., 2009; Harwood and Batista, 2008), PI3K catalyzes the phosphorylation of phosphatidylinositol-4,5-bisphosphate (PIP_2) to phosphatidylinositol-3,4,5-trisphosphate (PIP_3) at the plasma membrane. Bruton's tyrosine kinase (Btk), phospholipase-γ2 (PLC-γ2), and the serine/threonine kinase Akt/PKB are among proteins containing pleckstrin-homology (PH) domains, that are recruited to the plasma membrane after the generation of PIP_3 (Anderson et al., 1998; Deane and Fruman, 2004). The lipid phosphatase Pten (phosphatase and tensin homolog) counteracts PI3K activity and dephosphorylates PIP_3 to PIP_2 (Leslie and Downes, 2002; Maehama and Dixon, 1998). In early B cells, PI3K controls *immunoglobulin* (*Ig*) gene recombination, and later in development, PI3K signaling regulates the survival of mature cells and their fate upon activation by influencing their program of differentiation (Omori et al., 2006; Srinivasan et al., 2009). In line with this finding, enhanced PI3K activity blocks class-switch recombination (CSR) and activates the formation of plasma cells (Omori et al., 2006; Suzuki et al., 2003). Since plasma cell differentiation is mediated by the transcriptional suppressor Blimp-1 (Shaffer et al., 2002; Shapiro-Shelef et al., 2003), these data suggest that deregulated PI3K activity results in Blimp-1 activation and subsequent differentiation into plasma cells. In fact, Pten-deficient B cells are prone to undergo differentiation into plasma cells that secrete antibodies of the IgM isotype, as shown by highly elevated serum concentrations of IgM and reduced levels of IgA and IgG (Omori et al., 2006; Suzuki et al., 2003). Moreover, inactivation of Pten at later stages of B cell development leads to an increased population of CD5-positive B cells known as B-1a B cells, which express autoreactive BCR specificities. BCR activation is considered to be important for the development and maintenance of several non-Hodgkin lymphomas (NHLs) including chronic lymphocytic leukemia (CLL) (Chiorazzi et al., 2005; Seifert et al., 2012; Stevenson and Caligaris-Cappio, 2004). The importance of BCR activation and the downstream PI3K pathway for the malignant transformation of B cells is further supported by the fact that inhibitors for Btk or PI3K show effective therapeutic responses (Chang and Kahl, 2014; Spaargaren et al., 2015). However, mice with B-cell-specific inactivation of Pten show no development of B cell lymphomas unless an additional phosphatase, Ship-1, is inactivated (Miletic et al., 2010). Thus, an important question is why Pten deficiency as such is not sufficient for the development of lymphoproliferative disease despite the presence of B cells expressing autoreactive BCRs and possessing deregulated PI3K activity.

Here, we test the hypothesis that activated B cells are disposed to Blimp-1-mediated terminal differentiation at all stages of development and, therefore, constitutive BCR engagement is not sufficient for induction of uncontrolled B cell expansion.

RESULTS

Reduced BCR Expression and Altered B Cell Compartments in *Pten*-Deficient B Mice

Our previous experiments showed that inactivating the gene encoding Pten in pro-B cells using mb1-cre results in defective *Ig* gene recombination and a severe block at the pro-B cell stage (Alkhatib et al., 2012). Spleens from $Pten^{f/f}$ × mb1-cre mice exhibit only small follicles lacking IgM^+ cells, while the follicles

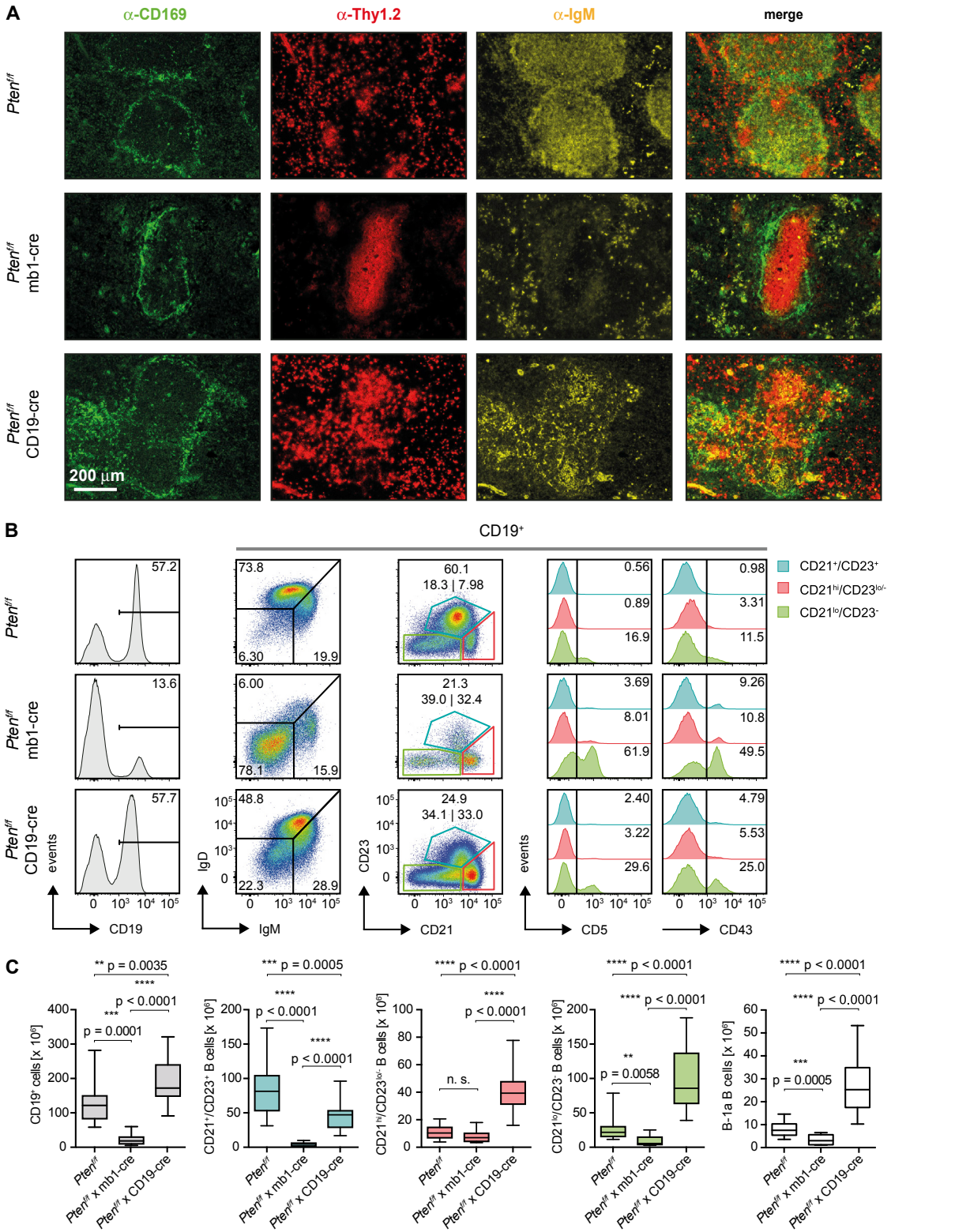

Figure 1. Reduced BCR Expression and Altered B Cell Compartments in Pten-Deficient Mice

(A) Immunohistochemistry staining of spleen sections from control, *Pten*$^{f/f}$ × mb1-cre and *Pten*$^{f/f}$ × CD19-cre mice for CD169 (green), Thy1.2 (red), and IgM (yellow) at 10× magnification. Shown pictures are representative of 2 mice per genotype.

(legend continued on next page)

in the spleens of *Pten*$^{f/f}$ × CD19-cre mice show an abnormal distribution of IgM^{+} cells compared with control mice (Figure 1A). More detailed analysis revealed that some peripheral B cells exist in *Pten*$^{f/f}$ × mb1-cre mice and that, based on fluorescence-activated cell sorting (FACS) staining for markers such as CD21 and CD23, cells corresponding to marginal zone B cells (MZ.B; CD21^{hi}/CD23$^{lo/-}$) or follicular B cells (Fo.B; CD21^{+}/CD23^{+}) can be found in these mice (Figure 1B). Moreover, an increased population of CD21^{lo}/CD23^{-} B cells was also detected in the spleens of *Pten*$^{f/f}$ × mb1-cre mice (Figure 1B). This enlarged CD21^{lo}/CD23^{-} population contains transitional B cells but also seems to consist of B-1a B cells, which are characterized by CD5 and CD43 expression (Figure 1B) (Piatelli et al., 2003) and partial reactivity to phosphatidylcholine (PtC) (Figure S1A) (Mercolino et al., 1988; Tsiantoulas et al., 2013). This is similar to the *Pten*$^{f/f}$ × CD19-cre mice that were previously shown to possess increased numbers of B-1a B cells (Figures 1B and 1C) (Suzuki et al., 2003). As compared to *Pten*$^{f/f}$ × CD19-cre mice, however, the majority of peripheral B cells in *Pten*$^{f/f}$ × mb1-cre mice showed reduced IgM expression and no IgD (Figures 1B and S1B), whereas IgD-positive cells were detected in *Pten*$^{f/f}$ × CD19-cre mice (Figure 1B). This difference might be caused by the developmental stage at which *Pten* was deleted in the different mouse strains. Indeed, due to differential gene expression of CD19 and mb1, CD19-cre acts at later stages of B cell development than mb1-cre, which acts prior to *Ig* gene recombination. It is conceivable that in B cells derived from *Pten*$^{f/f}$ × CD19-cre mice, *Pten* gene inactivation occurs after *Ig* gene recombination, and this might be the reason for the increased numbers of B cells in the spleens of *Pten*$^{f/f}$ × CD19-cre mice compared with *Pten*$^{f/f}$ × mb1-cre mice (Figure 1B-C). These data suggest that regulation of PI3K activity is required for early stages of B cell development and proper selection of B cells into distinct B cell populations. Combining autoreactive BCRs with *Pten* deficiency did not lead to abnormal expansion of any B cell subsets (data not shown), suggesting that autoreactive BCR specificity, together with constitutive activation of PI3K signaling, is not sufficient for uncontrolled proliferation of B cells.

B Cells from Pten-Deficient Mice Are Committed to Terminal Differentiation

In agreement with previous reports (Omori et al., 2006; Suzuki et al., 2003), we found that loss of Pten function in B cells, and thus increased PI3K activity, promotes plasma cell differentiation (Figure 2A). Although the percentage of plasma cells was low, B cells from Pten-deficient mice exhibited prior to stimulation an enhanced basal activity of mTor (mammalian target of rapamycin) as measured by S6 phosphorylation, and elevated levels of the transcription factors Irf4 and Blimp-1 compared to wild-type (WT) cells (Figures 2B and 2C). Three days upon stimulation with lipopolysaccharide (LPS), these factors were further elevated, while inhibitory factors such as Irf8, Bcl6, and Bach2 showed only slight changes (Figures 2B, 2C, S1C, and S1D). Foxo1 expression was specifically downregulated in CD138^{+} B cells in control and Pten-deficient mice (Figures S1C and S1D). These findings indicate that elevated PI3K activity leads to basal activation of mTor, Irf4, and Blimp-1, which initiates terminal differentiation of B cells.

In fact, we detected an increased population of CD138^{+}/B220^{lo} plasma cells specifically within the population of CD21^{lo}/CD23^{-} B cells in the spleens of *Pten*$^{f/f}$ × mb1-cre mice (Figure S2A), suggesting that CD21^{lo}/CD23^{-} cells are particularly prone to undergo terminal differentiation. To further investigate this, we stimulated sorted B cells from all three compartments (Fo.B CD21^{+}/CD23^{+}, MZ.B CD21^{hi}/CD23$^{lo/-}$, and CD21^{lo}/CD23^{-} B cells) with LPS (Figure S2B) and observed that B cells originating from the CD21^{lo}/CD23^{-} population readily differentiated into plasma cells. This behavior was most evident in B cells from *Pten*$^{f/f}$ × CD19-cre mice (Figure S2B). Moreover, the CD21^{lo}/CD23^{-} B cells, which are increased in *Pten*$^{f/f}$ × mb1-cre and *Pten*$^{f/f}$ × CD19-cre mice, express the highest levels of *Blimp-1* among the B cell populations (Figure 2D; for the gating strategy and re-analysis, see Figures S3A and S3B). The increased *Blimp-1* expression suggested that B cells with increased PI3K activity develop into a specific compartment that is committed to terminal differentiation under normal conditions. Accordingly, developing B cells that interact with auto-antigen may induce BCR-dependent PI3K signaling and become selected into this compartment. Indeed, the sera of *Pten*$^{f/f}$ × mb1-cre mice, despite having decreased B cell numbers and a slightly reduced concentration of IgM, contain increased amounts of autoreactive IgM (Figure 2E).

Together, our results suggest that Pten deficiency is associated with enhanced development of autoreactive B cells and elevated Blimp-1 activity, leading to increased terminal differentiation and secretion of autoreactive antibodies.

Increased Autoreactivity in *Prdm1*-Deficient B Cells

To directly test the role of Blimp-1 in early B cell selection, we performed a comprehensive analysis of B cell development in *Prdm1*$^{f/f}$ × mb1-cre mice. The early expression of mb1 in pro-B cells ensures efficient deletion of *Prdm1* at the earliest stages prior to VDJ recombination. The total number of B cells in the spleens of *Prdm1*$^{f/f}$ × mb1-cre mice were comparable to control mice, as were the amounts of Fo.B (CD21^{+}/CD23^{+}) and MZ.B (CD21^{hi}/CD23$^{lo/-}$) cells (Figures 3A, 3B, and S4A). However, the compartment of CD21^{lo}/CD23^{-} B cells was significantly increased (Figure S4A), and a distinct CD23^{-} population with

(B) Representative flow cytometric analysis of splenocytes from mice of the indicated genotypes for expression of BCR (IgM/IgD), CD23, and CD21. Histograms compare CD5 and CD43 expression in the different B cell subpopulations (pre-gated on CD19^{+} cells): follicular B cells (Fo.B; CD21^{+}/CD23^{+}, blue), marginal zone B cells (MZ.B; CD21^{hi}/CD23$^{lo/-}$, red), and CD21^{lo}/CD23^{-} B cells (green). Representative data of at least 8 mice per genotype are shown. Numbers in dotplots and histograms indicate the percentages of positive cells in the respective gates.
(C) Absolute cell numbers of total B cells (gray, left), Fo.B (blue), MZ.B (red), CD21^{lo}/CD23^{-} (green), and B1-a B cells (white, right) in spleens from control (n = 25), *Pten*$^{f/f}$ × mb1-cre (n = 8) and *Pten*$^{f/f}$ × CD19-cre mice (n = 18). Central horizontal line in the box represents the median, the upper and lower boundaries of the box show the respective quartile, and whiskers indicate the range of individual data.
See also Figure S1.

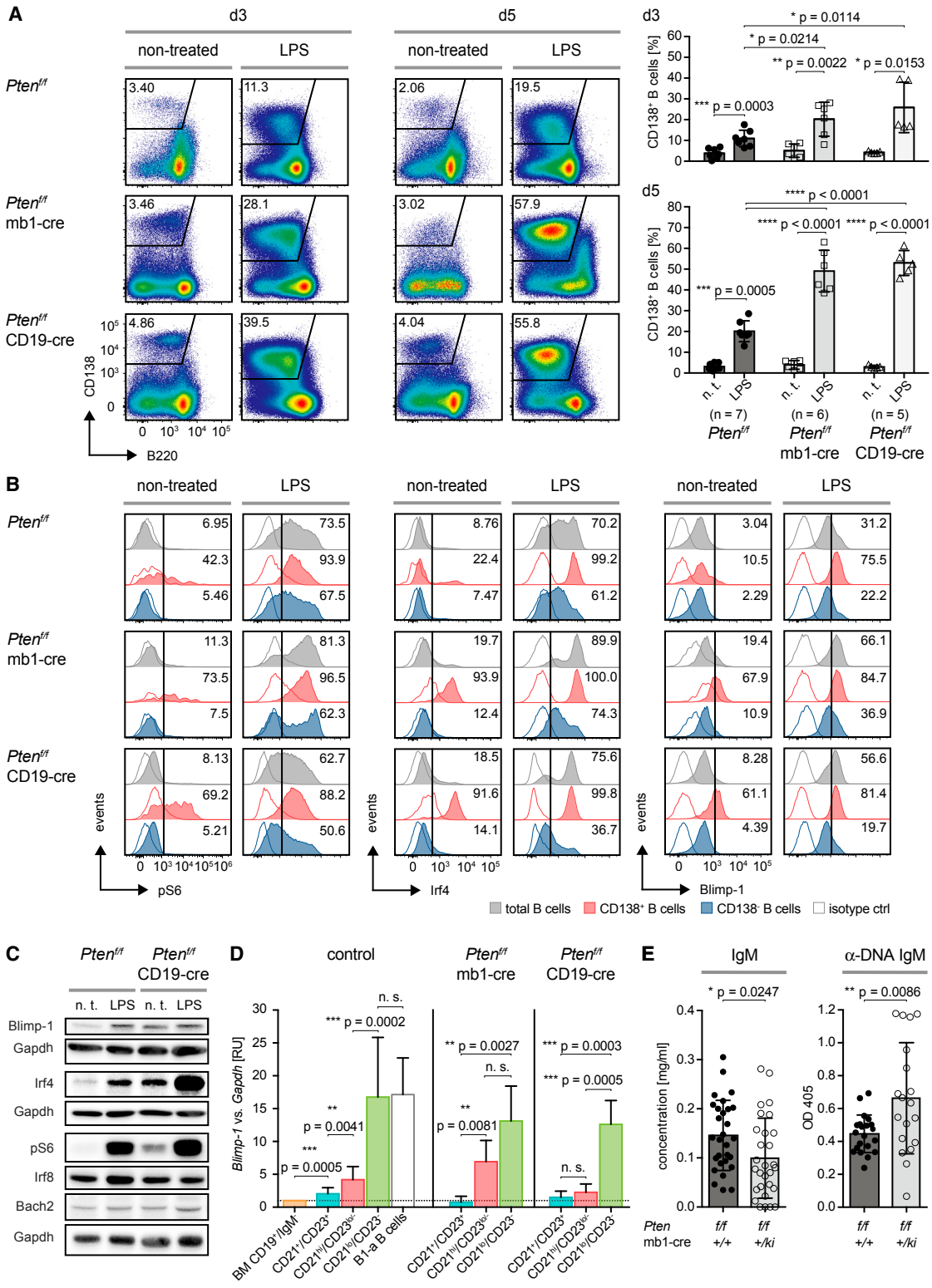

Figure 2. B Cells from Pten-Deficient Mice Are Committed to Terminal Differentiation

(A) Splenocytes from mice of the indicated genotypes were left untreated (n. t. = non-treated) or stimulated with 2.5 μg/mL LPS and analyzed after 3 and 5 days for B220 and CD138 expression by flow cytometry (pre-gated on $CD19^+$ cells). Bar diagrams besides the representative FACS plots show quantification of

(legend continued on next page)

intermediate CD21 expression (Figure 3A) was detected. Such a population was previously shown to contain $CD5^+$ B cells and to correlate with the production of autoantibodies (Nguyen and Baumgarth, 2016). In fact, the ratio and total cell number of B-1a B cells were increased in the absence of Blimp-1 (Figures 3A, 3B, S4B, and S4C). The increased $CD5^+$ B cell population was also observed after inducible deletion of *Prdm1 in vivo* (Figure S4D), suggesting that the absence of antibodies in the sera of $Prdm1^{f/f}$ × mb1-cre mice is unlikely the main reason for the expansion of B-1 cells in these mice. This finding indicates that Blimp-1 deficiency is associated with defects in B cell selection, thereby leading to increased numbers of potentially autoreactive B cells, as B-1a B cells often express autoreactive BCRs. To further test this, we determined the fraction of PtC-reactive B cells, since PtC is a common autoantigen recognized by B-1a BCRs (Mercolino et al., 1988; Tsiantoulas et al., 2013). PtC-reactive B cells were significantly increased in $Prdm1^{f/f}$ × mb1-cre mice compared to control mice (Figures 3A, S4C, and S4E). To confirm that Blimp-1 deficiency leads to the development of autoreactive B cells, we tested the antibody that might potentially be secreted by Blimp-1-deficient B cells. To this end, we introduced Blimp-1 by retroviral transduction into splenic $Prdm1^{f/f}$ × mb1-cre B cells and measured the concentration of secreted anti-dsDNA-IgM antibody in the supernatant after 7 days of stimulation with LPS to induce terminal differentiation (Figure 3C). Our results show that the supernatant of B cells derived from $Prdm1^{f/f}$ × mb1-cre mice contains significantly higher anti-dsDNA-IgM antibodies than control supernatants (Figure 3D).

This points toward an unexpected role of Blimp-1 in early B cell development. Accordingly, B cells that fail to remove an autoreactive BCR specificity undergo Blimp-1-induced premature terminal differentiation. To test this directly, we expressed the heavy (HC) and light chain (LC) of the hen-egg-lysozyme (HEL)-specific BCR (HH10) and the 4-Hydroxy-3-iodo-5-nitrophenylacetyl hapten (NIP)-specific B1-8 BCR in *Rag2*/*λ5*-double knockout (DKO) pro-B cells (Figure 3E) and tested induction of Blimp-1 expression after incubation with the cognate antigen or anti-BCR antibodies. In fact, treatment with antigen (HEL for HH10 and NIP(7)-BSA for B1-8 BCR, respectively) or anti-LC antibody led to upregulation of Blimp-1 (Figures 3F and 3G), and BCR-expressing cells were lost after incubation with these stimuli (Figures 3H and 3I). To show that Blimp-1 induction leads to negative selection *in vitro*, we transduced the *Rag2*/*λ5*-DKO with a *Blimp-1*-IRES-GFP retroviral vector and analyzed cell survival by monitoring GFP expression. We found that the majority of Blimp-1-expressing cells were lost within 2 days of culture as compared to cells transduced with the empty vector (EV) (Figure S4F). In summary, these results indicate that BCR engagement at early B cell developmental stages induces Blimp-1 expression and leads to premature differentiation, thereby preventing further development of autoreactive B cells.

These data suggest that defective Blimp-1 function leads to the development of autoreactive B cells and an increased compartment of B-1a B cells. However, Blimp-1 deficiency as such is not sufficient to induce uncontrolled proliferation of B cells.

Bcl2 Protects from Blimp-1-Mediated Cell Death

Previous findings indicated that anti-apoptotic factors can rescue cells from Blimp-1-mediated cell death (Hug et al., 2014; Knödel et al., 1999). Since our data indicate a role of Blimp-1 in early B cell development, we further analyzed the expression levels of *Blimp-1* and *Bcl2* in pro-B, small pre-B, and immature B cells from control mice (Figure 4A; for the gating strategy and re-analysis, see Figures S3C and S3D). In fact, *Blimp-1* expression is elevated in small-pre-B cells. This finding is further supported by published gene expression data showing that *Blimp-1* is upregulated at the fraction D of non-cycling pre-B cells (Figure S4G) (Bagger et al., 2016; Heng et al., 2008; Painter et al., 2011). At this stage, B cells rearrange the *Ig LC* gene and undergo selection for BCR function. Although *Blimp-1* expression is low compared to plasma cells (Figure 4A; for the gating strategy and re-analysis, see Figure S3E), the expression level is comparable to immature or mature Fo.B cells (Figures 4A and S4G).

Since later stages of development such as Fo.B cells or B-1a cells also express higher levels of *Bcl2* than early cells or $CD21^{lo}$/$CD23^-$ B cells (Figures 4B and S4G; for the gating strategy and re-analysis, see Figures S3A, S3B, and S3F), it is conceivable that the increased Bcl2 protects these cells from Blimp-1-mediated premature differentiation. Interestingly, the $CD21^{lo}$/$CD23^-$ population in $Pten^{f/f}$ × $Prdm1^{f/f}$ × CD19-cre mice shows significantly higher *Bcl2* expression (Figure 4B).

To show that *Blimp-1* expression leads to cell death *in vitro* unless cells are protected by anti-apoptotic factors, we transduced *Rag2*/*λ5*-DKO concomitantly with retroviral expression vectors for Blimp-1 and Bcl2 and analyzed cell survival by monitoring the fluorescence of the respective reporter. We found that the majority of Blimp1-expressing cells were lost within a few days of culture compared to cells transduced with the empty vector (Figures 4C and 4D). Only cells that were transduced

$CD138^+$ B cells in LPS- and non-treated splenocytes at days 3 (top) and 5 (bottom) post stimulation. $Pten^{f/f}$ (n = 7), $Pten^{f/f}$ × mb1-cre (n = 6) and $Pten^{f/f}$ × CD19-cre mice (n = 5), mean ± SD. Statistical significance was calculated by using the two-tailed paired (n. t. versus LPS) and otherwise the two-tailed unpaired t test.

(B) Intracellular flow cytometric analysis of pS6, Irf4, and Blimp-1 expression in splenocytes from Figure 2A at day 3. Numbers in the histogram plots indicate the percentages of positive cells. Data are representative of at least 2 mice per genotype.

(C) Immunoblot analysis of Blimp-1, Irf4, pS6, Irf8, and Bach2 expression in splenocytes from Figure 2A at day 3. n. t. = non-treated; Gapdh served as loading control. Data are representative of at least 2 mice per genotype.

(D) Fo.B ($CD21^+$/$CD23^+$, blue), MZ.B ($CD21^{hi}$/$CD23^{lo/-}$, red), and $CD21^{lo}$/$CD23^-$ B cells (green) from control (n = 11), $Pten^{f/f}$ × mb1-cre (n = 5) and $Pten^{f/f}$ × CD19-cre mice (n = 4) were FACS-purified (for the gating strategy and re-analysis, see Figures S3A, S3B, and S3F) and expression levels of *Blimp-1* in the respective B cell populations were determined by quantitative reverse transcriptase (RT)-PCR. Results are shown as relative units (RU) normalized to levels measured in bone-marrow (BM)-derived pro-B cells ($CD19^+$/$B220^+$/IgM^-/IgD^-/$CD25^-$), mean + SD.

(E) Concentrations of IgM in the sera of $Pten^{f/f}$ and $Pten^{f/f}$ × mb1-cre mice were measured by α-IgM ELISA, (n = 29; mean ± SD) (left). Levels of autoreactive antibodies in the respective sera were determined by α-dsDNA-IgM ELISA ($Pten^{f/f}$, n = 21; $Pten^{f/f}$ × mb1-cre, n = 19; mean ± SD) (right).

See also Figures S1–S3.

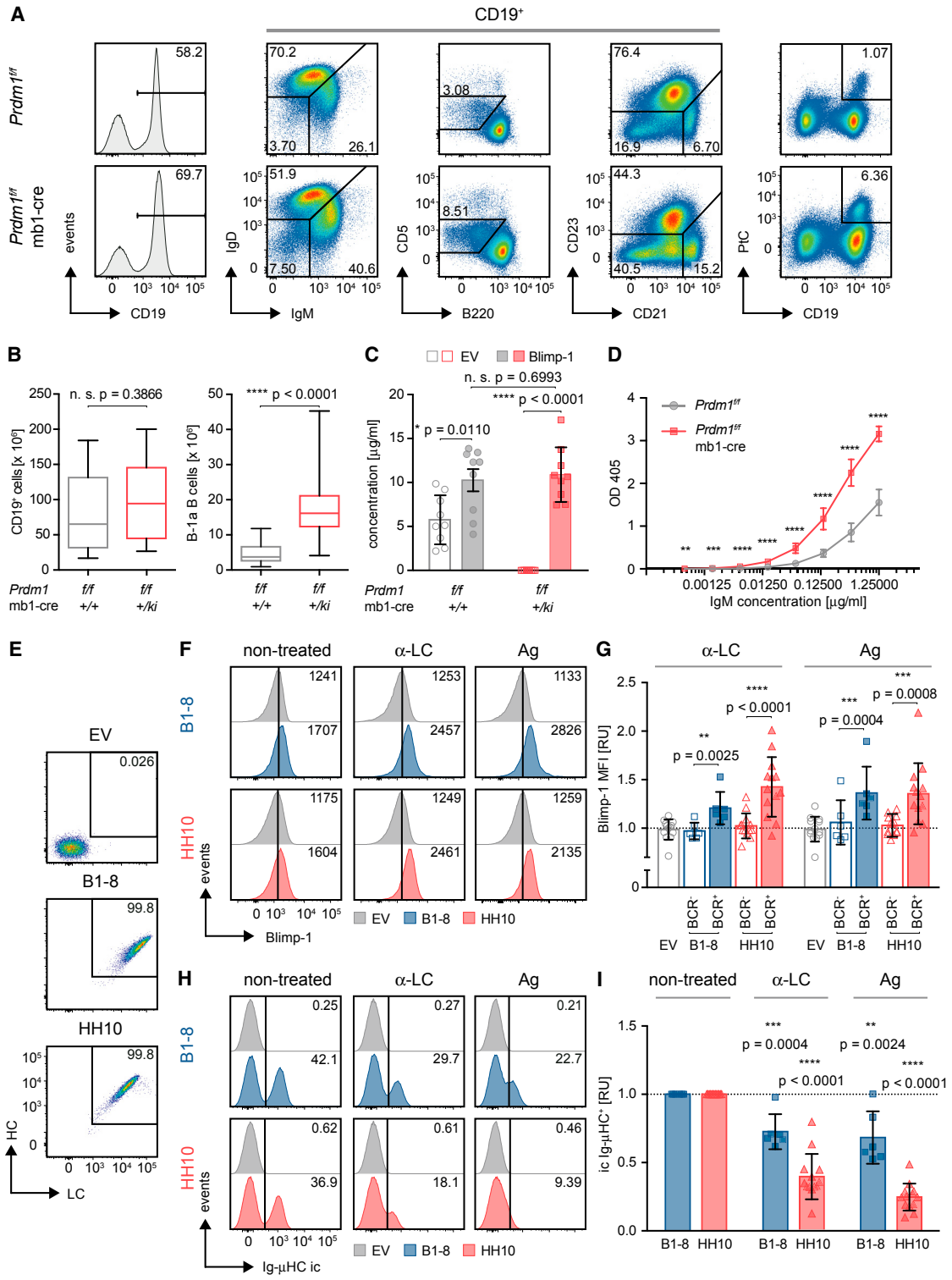

Figure 3. Increased Autoreactivity in Blimp-1-Deficient B Cells

(A) Splenocytes from *Prdm1*$^{f/f}$ and *Prdm1*$^{f/f}$ × mb1-cre mice were analyzed by flow cytometry for surface expression of the indicated markers and reactivity to phosphatidylcholine (PtC).

(B) Absolute numbers of total B cells and B-1a B cells in spleens from *Prdm1*$^{f/f}$ x mb1-cre mice compared to controls (n = 14, median ± quartile and range).

(legend continued on next page)

with both Bcl2 and Blimp-1 were protected from Blimp-1-mediated cell death (Figures 4C and 4D). Blimp-1-transduced cells showed reduced mTor activity (Figure S4H) and an impaired cell cycle (Figure 4E) and were more prone to apoptosis compared to cells transduced with the empty vector (Figure 4F). In the presence of Bcl2, Blimp-1-transduced cells were protected from apoptosis induced by premature terminal differentiation (Figure 4F).

Together, these results suggest that Blimp-1 can be induced already at early stages of B cell development, thereby leading to cell death by premature activation of the terminal differentiation program, which can be blocked by concomitant expression of anti-apoptotic factors.

Premature Terminal Differentiation Prevents Uncontrolled Proliferation

Since increased PI3K activity induces Blimp-1, it is conceivable that induction of Blimp-1 may prevent the proliferation or survival of B cells with constitutive BCR signaling. In fact, Pten-deficient B cells show a moderate increase of B-1a B cells but normally no tumor development despite sustained PI3K activation (Figure S5A). To investigate how Blimp-1 induction in Pten-deficient B cells prevents B cell expansion, we performed a detailed analysis of the *Pten*$^{f/f}$ × *Prdm1*$^{f/f}$ × CD19-cre mice. These mice show an increased B-1a B cell compartment already at 7 and splenomegaly at 15 weeks of age (Figures S5A and 5A). Besides the increased population of B-1a cells showing a B220^{lo}/CD5$^{int/+}$ phenotype, T cells (B220^{-}/CD5^{hi}) and conventional B-2 B cells (B220^{+}/CD5^{-}) can be detected in the spleens of *Pten*$^{f/f}$ × *Prdm1*$^{f/f}$ × CD19-cre mice (Figure 5B). The phenotype of B-1a cells was confirmed by further analysis of the B220^{lo}/CD5$^{int/+}$ population revealing that these cells, similar to B-1a B cells, are CD19^{+}/B220^{lo}/CD5^{+}/IgM^{+}/IgD^{lo}/CD23^{-}/CD21^{lo} and partially reactive to PtC (Figure S5B). Moreover, their numbers are dramatically increased in all lymphoid organs of the *Pten*$^{f/f}$ × *Prdm1*$^{f/f}$ × CD19-cre mice (Figures 5B–5F and S5B; data not shown). Since the CD21^{lo}/CD23^{-} B cell population contains the B1-a B cells, which show higher *Bcl2* expression and accumulate in *Pten*$^{f/f}$ × *Prdm1*$^{f/f}$ × CD19-cre mice, this might also be the reason for the significant increase of *Bcl2* expression in this population and group of mice (Figure 4B). Spleen sections showed an increased population of B cells with high IgM expression in the follicles of the respective mice (Figure 5G). To assess whether this prominent population of B-1a cells represents a transformed population with a clonal BCR, we analyzed the V(D)J usage in the CD19^{+}/CD5^{+} population of the *Pten*$^{f/f}$ × *Prdm1*$^{f/f}$ × CD19-cre splenic B cells (Figure S5D; Table S7). However, we detected merely random combinations of gene segments, suggesting that this population consists of a multitude of individual B cells. Together, our results suggest that the induction of Blimp-1 is an important mechanism for the prevention of uncontrolled B cell activation and expansion under conditions of constitutive BCR signaling.

Reconstitution of Blimp-1 Activates Terminal Differentiation

To confirm that the increased proliferation of *Pten*$^{f/f}$ × *Prdm1*$^{f/f}$ × CD19-cre B cells is caused by defective terminal differentiation of activated B cells, we investigated plasma cell differentiation in *Pten*$^{f/f}$ × *Prdm1*$^{f/f}$ × CD19-cre B cells. We found that splenic B cells from *Pten*$^{f/f}$ × *Prdm1*$^{f/f}$ × CD19-cre mice were defective in plasma cell differentiation (Figures 6A and 6B) and showed an enhanced survival capacity upon stimulation with LPS *in vitro* (Figure S6A). In line with the *in vivo* data, Blimp-1 deficiency resulted in extended survival of CD21^{lo}/CD23^{-} B cells, but not CD21^{+}/CD23^{+} Fo.B cells, *in vitro* (Figures 6C and S5B).

As expected, when Blimp-1 expression was reconstituted by retroviral transduction, *Pten*$^{f/f}$ × *Prdm1*$^{f/f}$ × CD19-cre B cells showed efficient plasma cell differentiation (Figure 6D). Interestingly, Blimp-1 expression resulted in downregulation of the pro-survival factor Bcl2 (Figure 6E) and respective cells were rapidly lost *in vitro* (Figure 6F).

While most B cells are BCR-negative in the spleens of *Pten*$^{f/f}$×mb1-cre mice, the block was partially rescued in *Pten*$^{f/f}$ × *Prdm1*$^{f/f}$ × mb1-cre mice, resulting in a large fraction of cells expressing IgM BCR (Figures 6G, S6C, and S6D). This suggests that Blimp-1-mediated premature terminal differentiation results in the removal of the vast majority of BCR expressing Pten-deficient early B cells. Together, these data indicate that sustained BCR signaling and deregulated PI3K activity result in Blimp1-mediated terminal differentiation of B cells, thereby interfering with early B cell selection and expansion of peripheral B cells.

(C) *In vitro* antibody secretion by mature splenic B cells from mice of the indicated genotypes after retroviral transduction with the empty vector (EV) or an expression vector encoding Blimp-1 was measured by α-IgM ELISA (n = 9, mean ± SD). Statistical significance was calculated using a two-tailed paired t test (between EV and Blimp-1) or a two-tailed unpaired t test (between *Prdm1*$^{f/f}$ and *Prdm1*$^{f/f}$ × mb1-cre).

(D) The autoreactive capacity of antibody secreted *in vitro* by splenocytes from mice of the indicated genotypes was determined by α-dsDNA ELISA (n = 9, mean ± SD). IgM concentrations used in the α-dsDNA ELISA were calculated based on the results shown (C), assuming that Blimp-1-reconstituted *Prdm1*$^{f/f}$ and *Prdm1*$^{f/f}$ × mb1-cre cells show similar concentrations.

(E) Representative analysis of BCR expression in *Rag2*/*λ5*-double-knockout (DKO) pro-B cells reconstituted with heavy and light chain of NIP-(B1-8, middle) and hen-egg-lysozyme (HEL)-specific (HH10, bottom) IgM BCR or EV (top), respectively.

(F) *Rag2*/*λ5*-DKO expressing either B1-8 (blue) or HH10 (red) BCR were mixed with untransduced (BCR-deficient) *Rag2*/*λ5*-DKO cells at a 1:1 ratio. Intracellular Blimp-1 expression levels were measured in BCR^{+} and BCR^{-} populations (defined by intracellular Ig-μHC staining) following 38 hr of incubation with anti-BCR antibodies (0.5 μg/mL α-λ or α-κLC, respectively) or the cognate antigen (Ag; 50 ng/mL NIP(7)-BSA or soluble HEL, respectively).

(G) Quantification of the MFI of Blimp-1 (in the cells from F) normalized to the respective unstimulated control (EV, n = 13; B1-8$^{+/-}$, n = 6; HH10$^{+/-}$, n = 13; mean ± SD). Statistical significance was calculated using a two-tailed paired t test.

(H) Percentages of viable Ig-μHC^{+} (intracellular [ic]) cells following 38 hr of stimulation with an α-LC antibody or the cognate antigen (as described in F).

(I) Quantification of percentages of viable ic Ig-μHC^{+} cells (cells from H) normalized to the respective unstimulated control (EV, n = 13; B1-8$^{+/-}$, n = 6; HH10$^{+/-}$, n = 13; mean ± SD). Statistical significance was calculated compared to non-treated samples using a two-tailed paired t test.

See also Figure S4.

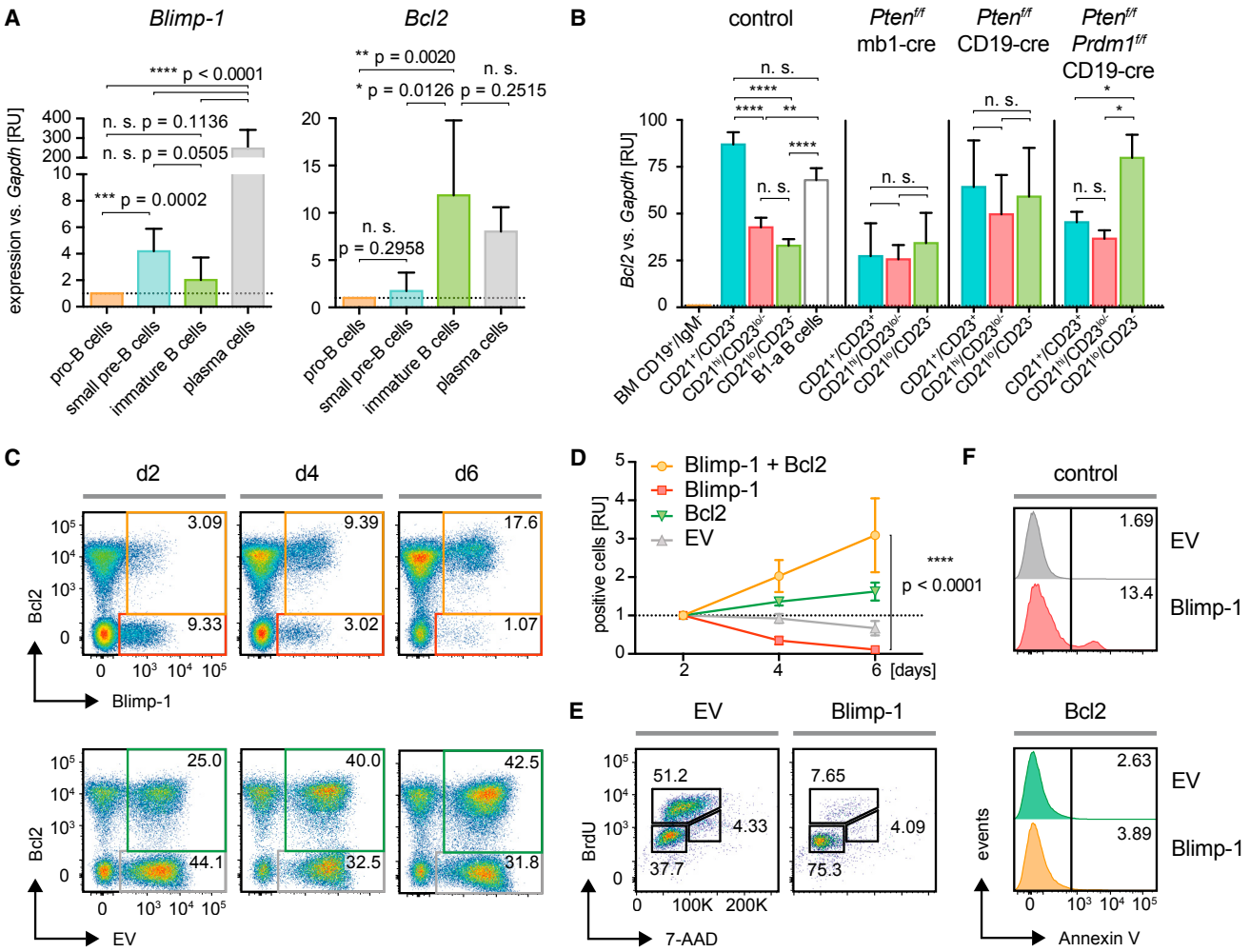

Figure 4. Bcl2 Protects from Blimp-1-Mediated Cell Death

(A) Pro-B cells (CD19$^+$/B220$^+$/IgM$^-$/IgD$^-$CD25$^-$, orange, n = 6), small pre-B cells (CD19$^+$/B220$^+$/IgM$^-$/IgD$^-$/CD25$^+$, blue, n = 6), and immature B cells (CD19$^+$/B220$^+$/IgM$^+$/IgD$^-$/CD25$^-$, green, n = 6) from control mice were FACS-purified (for the gating strategy and re-analysis, see Figures S3C–S3E), and expression levels of *Bcl2* and *Blimp-1* in the respective populations are shown as RU to the levels measured in pro-B cells. Expression levels are shown in comparison to FACS-purified plasma cells (gray, n = 7), mean + SD.

(B) Splenic Fo.B (CD21$^+$/CD23$^+$, blue), MZ.B (CD21^{hi}/CD23$^{lo/-}$, red), CD21^{lo}/CD23$^-$ B cells (green), and B1-a B cells (control only, n = 6, gray) from control (n = 11), *Pten*$^{f/f}$ × mb1-cre (n = 3), *Pten*$^{f/f}$ × CD19-cre (n = 4) and *Pten*$^{f/f}$ × *Prdm1*$^{f/f}$ × CD19-cre mice (n = 4) were FACS-purified (for the gating strategy and re-analysis, see Figures S3A, S3B, and S3E), and expression levels of *Bcl2* in the respective B cell populations were determined by quantitative RT-PCR. Results are shown as RU normalized to levels measured in bone-marrow-derived pro-B cells (mean + SD).

(C) Representative flow cytometric analysis data from concomitant expression of Bcl2 and Blimp-1 (top) or the EV (bottom) in *Rag2*/*λ5*-DKO pro-B cells, respectively, measured at days 2, 4, and 6 after transduction.

(D) Quantified percentages of viable GFP$^+$ (Bcl2) and/or Berry$^+$ (Blimp-1 or EV, respectively) cells in the respective quadrants from Figure 6C at days 4 and 6 were normalized to the percentages measured at day 2 after transduction (right panel, n = 12, mean ± SD). Statistical significance was calculated using a two-tailed paired t test.

(E) Cell-cycle analysis in Blimp-1- and EV-transduced cells from Figures 6C and 6D.

(F) Measurement of apoptosis by staining for Annexin V in Blimp-1- and EV-transduced cells from Figures 6C–6E in absence (top) and presence (bottom) of Bcl2. See also Figures S3 and S4.

Transgenic *Bcl2* Causes Uncontrolled Expansion of Pten-Deficient Cells

The above findings suggest that constitutive BCR activation together with deregulated PI3K activity leads to Blimp-1-induced apoptosis, thereby preventing uncontrolled expansion of Pten-deficient B cells that express autoreactive BCR. To test whether ectopic overexpression of Bcl2 could protect Pten-deficient cells from Blimp-1-mediated cell death, we crossed *Pten*$^{f/f}$ × CD19-cre mice on a *Bcl2*-transgenic background. The resulting *Pten*$^{f/f}$ × CD19-cre × *Bcl2*^{tg} mice exhibit an extremely enlarged spleen and lymph nodes already at the age of 10 weeks as compared to age-matched *Pten*$^{f/f}$ × CD19-cre or *Bcl2*^{tg} controls (Figure 7A; data not shown). These mice were analyzed before 16 weeks of age, where signs of leukemic disease become

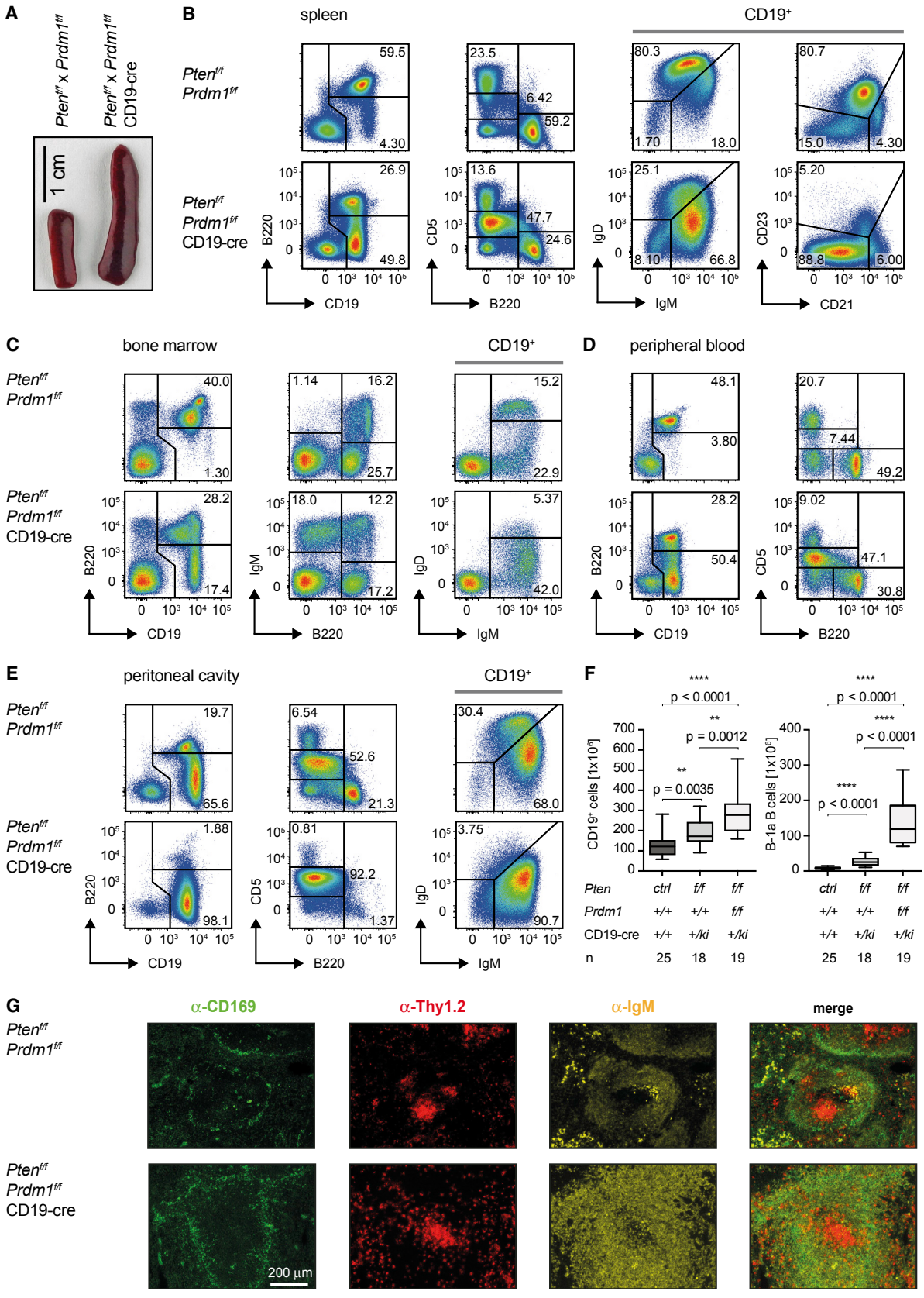

(legend on next page)

evident. We observed a dramatically increased compartment of total B cells ($CD19^+/B220^+$) in bone marrow, spleen, peritoneal cavity, peripheral blood, and lymph nodes (Figure 7A–7D; data not shown). Although the B-1a compartment is significantly increased (Figure 7B), the majority of expanded B cells did not exhibit a classical B-1a phenotype in the $Pten^{f/f}$ × CD19-cre × $Bcl2^{tg}$ mice (Figure 7D). In contrast to spleens from $Pten^{f/f}$ × $Prdm1^{f/f}$ × CD19-cre mice, the majority of B cells in these mice lack CD5 and surface BCR expression (Figure 7D). We compared the state of *Pten* deletion in the $IgM^{-/lo}/IgD^-$ and IgM^+/IgD^+ B cell subsets and found that *Pten* was deleted to comparable extent in both populations (Figure S7A). Since all surface $IgM^{-/lo}/IgD^-$ B cells showed intracellular Ig-μHC expression (Figure S7B), we assume that this population is composed of B cell precursors and plasma cells. In fact, we detected antibody secreting cells among the $IgM^{-/lo}/IgD^-$ population from $Pten^{f/f}$ × CD19-cre × $Bcl2^{tg}$ and $Pten^{f/f}$ × $Bcl2^{tg}$ mice (Figure 7E). In full agreement, analysis of serum Ig revealed that IgM is strongly elevated in these mice (Figure 7F) and that the population of $CD138^+/B220^{lo}$ plasma cells is enlarged in the spleens of $Pten^{f/f}$ × CD19-cre × $Bcl2^{tg}$ mice as compared to $Bcl2^{tg}$ mice (Figure 7G). In addition, a considerable proportion of the $IgM^{-/lo}/IgD^-$ population lacked LC expression while expressing Ig-μHC, suggesting that pre-BCR expression is involved in the expansion of these cells (Figure S7B).

Taken together, our results suggest that deregulated PI3K by Pten deficiency leads to activation-induced cell death at multiple stages of development and that rescuing from apoptosis results in abnormal expansion of corresponding cells. Moreover, Blimp-1-mediated premature terminal differentiation is required to prevent the generation and expansion of autoreactive B cells.

DISCUSSION

PI3K activity regulates B cell differentiation and the fate of developing B cells. In fact, chronic PI3K activation by deletion of *Pten* in the early stages of B cell development results in severe block due to defective *Ig* gene rearrangement (Alkhatib et al., 2012), whereas deleting *Pten* at later stages leads to alterations in the peripheral B cell compartments, such as increased generation of B-1 B cells and accelerated plasma cell differentiation (Omori et al., 2006; Suzuki et al., 2003), suggesting that the development of Fo.B cells is suppressed in the absence of Pten. Since B-1 B cells require increased signaling for their development, Pten deficiency might cause the outgrowth of B cells that are persistently activated by their autoreactive BCR specificities and eventually become B-1 B cells (Casola et al., 2004; Hoffmann et al., 2007; Jellusova et al., 2010; Nguyen et al., 2017).

However, persistent BCR activation and constitutive PI3K signaling through Pten deficiency are not sufficient for malignant transformation, as Pten deficiency interferes with B cell maturation, thereby promoting the program of terminal differentiation by activation of Blimp-1 expression. Most likely, the amount of anti-apoptotic factors, including Bcl2, determines the survival of Pten-deficient B cells, as Blimp-1 has been shown to suppress the expression of genes driving proliferation (Shaffer et al., 2002) and to interfere with Bcl2 expression (Hug et al., 2014). Therefore, we propose that induction of Blimp-1 prevents the expansion of activated B cells and that this occurs already at the early stages of development. In agreement with previous studies (Savage et al., 2017; Shapiro-Shelef et al., 2003, 2005), our data show that Blimp-1 deficiency results in changes in B-1a B cells and, unexpectedly, in increased development of autoreactive B cells.

Our study reports a role for Blimp-1 in negative selection of B lymphocytes, thereby pointing to an unexpected recapitulation of regulatory networks in B cell development. In accordance with previous studies (Tellier et al., 2016), LPS-induced plasma cell differentiation led to increased Blimp-1 expression and elevated S6 phosphorylation by mTor. However, overexpression of Blimp-1 by retroviral transduction in pro-B cells resulted in reduced pS6 levels, suggesting that the amount of Blimp-1 and the stage of development are important for the relationship between Blimp-1 expression and the regulation of mTor activity.

Importantly, the transcription factor Irf4, which is known to be crucial for *LC* gene recombination and to be required for plasma cell differentiation and CSR (Johnson et al., 2008; Klein et al., 2006; Meixlsperger et al., 2007; Muljo and Schlissel, 2003), seems to be involved in the Blimp-1-mediated premature terminal differentiation. In analogy to available data (Sciammas et al., 2006) showing that high Irf4 amounts induce Blimp-1 while intermediate levels of Irf4 induce AID, which is required for CSR, it is conceivable that intermediate levels of Irf4 at early stages of development activate Rag-mediated *LC* gene recombination while increased levels activate Blimp-1 that interferes with cell division and survival (Shaffer et al., 2002). Thus, the induction of Blimp-1 in B cells that express autoreactive BCRs or harbor mutations, such as Pten deficiency, represents a safeguard mechanism that prevents the development of autoreactive B cells and interferes with proliferation (Shaffer et al., 2002). In fact, our data show that Blimp-1 deficiency or combined deficiency of Pten and Blimp-1 leads to an increased proportion of autoreactive B cells and abnormal expansion of B-1a B cells, respectively. This suggests that Blimp-1 not only acts as tumor suppressor in B cells (Calado et al., 2010; Lenz and Staudt, 2010; Mandelbaum et al., 2010) it is also required for proper selection of antibody

Figure 5. Premature Terminal Differentiation Prevents Uncontrolled Proliferation

(A) Macroscopic appearance of spleens from control and $Pten^{f/f}$ × $Prdm1^{f/f}$ × CD19-cre mice.

(B–E) Freshly isolated cells from spleens (B), bone marrow (C), peripheral blood (D), and peritoneal cavities (E) of control and $Pten^{f/f}$ × $Prdm1^{f/f}$ × CD19-cre mice were analyzed by flow cytometry for surface expression of the indicated markers. Representative data are shown from at least 10 individual mice sacrificed and analyzed at the age of 16–20 weeks.

(F) Absolute numbers of $CD19^+$ and B-1a B cells in spleens from $Pten^{f/f}$ x $Prdm1^{f/f}$ x CD19-cre (n = 19, median ± quartile and range) compared to the cell numbers of $Pten^{f/f}$ x CD19-cre and control mice already shown in Figure 1C.

(G) Immunohistochemistry staining of spleen sections from mice of the indicated genotypes for CD169 (green), Thy1.2 (red), and IgM (yellow).

See also Figure S5.

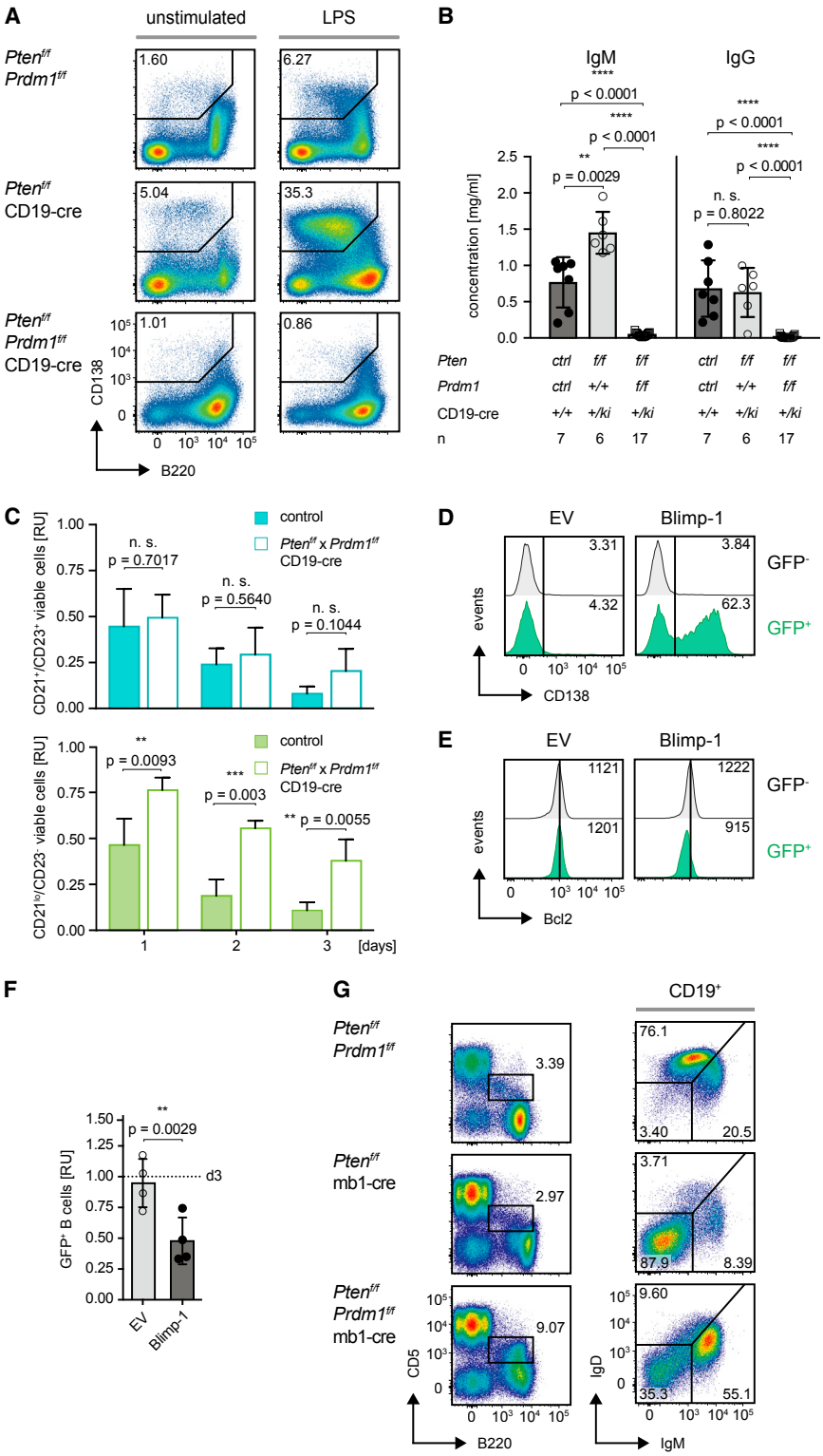

Figure 6. Reconstitution of Blimp-1 Activates Terminal Differentiation

(A) Splenocytes from mice of the indicated genotypes were stimulated with 2.5 μg/mL LPS and after 5 days analyzed for B220 and CD138 expression by flow cytometry.

(B) IgM and total IgG levels in sera from *Pten*$^{f/f}$ × *Prdm1*$^{f/f}$ × CD19-cre (n = 17), *Pten*$^{f/f}$ × CD19-cre (n = 6), and control mice (n = 7) (mean ± SD).

(C) Fo.B (CD21^{+}/CD23^{+}, top) and CD21^{lo}/CD23^{-} (bottom) splenic B cells from mice of the indicated genotypes were FACS-purified and cultured *in vitro*. The percentages of viable cells were monitored over 3 days, assessed by the morphology and staining with viability dye, and normalized to the percentage of viable cells at day 0 (n = 4, mean + SD).

(D) Analysis of CD138 expression in *Pten*$^{f/f}$ × *Prdm1*$^{f/f}$ × CD19-cre splenocytes 3 days following reconstitution with either Blimp-1 or EV by retroviral transduction. Histograms compare CD138 expression in GFP^{+} (Blimp-1-reconstituted) and GFP^{-} bystander cells. Numbers in the histogram plots indicate the percentages of CD138^{+} cells.

(E) Analysis of Bcl2 expression in cells described in Figure 5D. Histograms compare Bcl2 expression in GFP^{+} (Blimp-1-reconstituted) and GFP^{-} bystander cells.

(F) Splenocytes from *Pten*$^{f/f}$ × *Prdm1*$^{f/f}$ × CD19-cre mice were reconstituted either with EV or Blimp-1, and the percentages of GFP^{+} cells were measured at day 5 after transduction and normalized to the respective percentages measured 3 days after transduction (n = 4, mean ± SD).

(G) Splenocytes from *Pten*$^{f/f}$ × *Prdm1*$^{f/f}$ and *Pten*$^{f/f}$ × *Prdm1*$^{f/f}$ × mb1-cre mice were analyzed by flow cytometry for surface expression of the indicated markers. Data are representative of 2 individual mice sacrificed and analyzed at the age of 10 and 17 weeks.

Data shown in (D) and (E) are representative of two independent experiments. See also Figure S6.

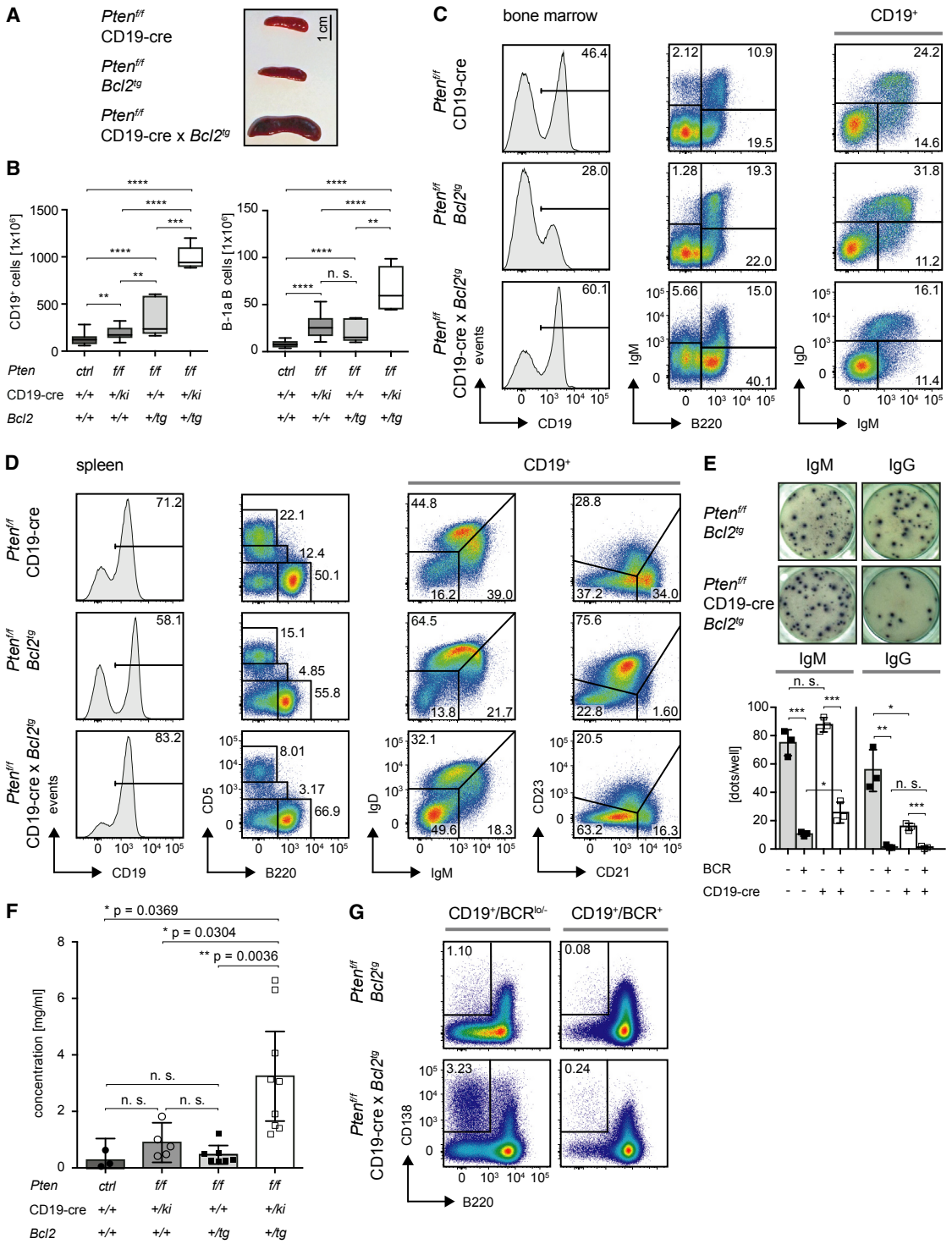

Figure 7. Transgenic *Bcl2* Causes Uncontrolled Expansion of Pten-Deficient B Cells

(A) Macroscopic appearance of spleens from *Pten*$^{f/f}$ × CD19-cre, *Pten*$^{f/f}$ × *Bcl2*^{tg}, and *Pten*$^{f/f}$ × CD19-cre × *Bcl2*^{tg} mice sacrificed at the age of 10 weeks.

(B) Absolute numbers of CD19^{+} and B-1a B cells in *Pten*$^{f/f}$ x CD19-cre x *Bcl2*^{tg} (n = 5) and *Pten*$^{f/f}$ x *Bcl2*^{tg} (n = 5) compared to the *Pten*$^{f/f}$ x CD19-cre and control mice already shown in Figures 1C and 5F (median ± quartile and range).

(C and D) Cells freshly isolated from spleens (C) and bone marrow (D) of *Pten*$^{f/f}$ × CD19-cre, *Pten*$^{f/f}$ × *Bcl2*^{tg}, and *Pten*$^{f/f}$ × CD19-cre × *Bcl2*^{tg} mice were analyzed by flow cytometry for surface expression of the indicated markers. Representative data are shown from at least 5 mice sacrificed and analyzed at the age of 10 weeks.

(legend continued on next page)

repertoire. Therefore, elucidating the signaling pathways that activate Blimp-1 is not only required for understanding plasma cell differentiation and the suppression of malignant transformation but also for understanding the molecular mechanisms that regulate the selection of developing B cells.

EXPERIMENTAL PROCEDURES

Mice

Pten$^{f/f}$ (provided by T. Mak; Campbell Family Institute for Breast Cancer Research at Princess Margaret Hospital, Toronto, ON, Canada; Suzuki et al., 2003) and *Prdm1*$^{f/f}$ (Shapiro-Shelef et al., 2003) mice were crossed either to mb1-cre (CD79a-cre) (Hobeika et al., 2006) or CD19-cre (Rickert et al., 1997) transgenic mice for B-cell-specific cre-mediated recombination. *Pten*$^{f/f}$ × CD19-cre mice were bred to either *Prdm1*$^{f/f}$ or *Bcl2*-transgenic mice (Strasser et al., 1991) in order to generate *Pten*$^{f/f}$ × *Prdm1*$^{f/f}$ × CD19-cre or *Pten*$^{f/f}$ × CD19-cre × *Bcl2*^{tg} mice, respectively. Male or female mice at 8 to 60 weeks of age were used in this study. Mice with WT, homozygous, or heterozygous floxed alleles for *Prdm1* or *Pten* were used as controls (*ctrl*).

Mice were bred and housed under specific-pathogen-free conditions in the animal facility of Ulm University. All animal experiments were done in compliance with the guidelines of the German law and approved by the Animal Care and Use Committees of Ulm University and the local government.

Cell Culture and Biochemistry

Phoenix and mature splenic B cells were cultured in Iscove's medium (Biochrom AG) containing 10% heat-inactivated fetal calf serum (FCS; PAN-Biotech), 2 mM L-glutamine, 100 U/mL penicillin (Gibco), 100 U/mL streptomycin (Gibco), and 50 μM β-mercaptoethanol (Gibco). *Rag2/λ5*-deficient cell lines were established by culturing bone marrow cells from the respective mice (Meixlsperger et al., 2007; Storch et al., 2007) in medium supplemented with the supernatant of J558L plasmacytoma cells stably transfected with a vector encoding murine IL-7. Cells were stimulated either with 0.5 μg/mL unlabeled α-kappa or α-lambda antibody (both polyclonal; Southern Biotech), 50 ng/mL soluble HEL (Sigma-Aldrich), or 50 ng/mL NIP(7)-BSA (Biosearch Technologies), respectively.

Plasmids and Retroviral Transduction

Full-length cDNA encoding Blimp-1 or Bcl2, respectively, was subcloned into the retroviral vector backbone pMI to generate *Blimp-1*-IRES-Berry, *Blimp-1*-IRES-GFP, and *Bcl2*-IRES-GFP expression vectors. Immunoglobulin HCs and LCs were expressed by using the BiFC vector system as described (Köhler et al., 2008). Viral supernatants were generated using the Phoenix retroviral producer cell line as described in the manufacturer's instructions. Phoenix cells were cultured in Iscove's culture medium + 10% FCS. Cells were plated at a density of 10^6 cells/mL to generate supernatants by using the transfection reagent GeneJuice (Merck Millipore). Retroviral supernatants were harvested after 48 hr. For the subsequent transduction, the respective cells were mixed with supernatants and centrifuged for 3 hr at 300 × *g* and 37°C. Transduced cells were cultured for 4–5 days and analyzed by flow cytometry.

Flow Cytometry

For flow cytometric analysis, cell suspensions were pretreated with α-CD16/CD32 Fc-Block (2,4G2; BD Biosciences) and stained by standard procedures. Dead cells were excluded by staining with Fixable Viability Dye eFluor 780 (eBioscience). Cells were stained using the antibodies listed in Table S1.

PtC-reactive cells were identified by staining with PtC-liposome fluorescein-DHPE (FormuMax Scientific). Biotin was detected by using Streptavidin Qdot 605 (Molecular Probes/Invitrogen). Unconjugated α-Pten- and α-Foxo1 antibodies were detected by using α-rabbit IgG (H+L) F(ab′)$_2$ fragment-Alexa Fluor 647 (Cell Signaling). Intracellular flow cytometric staining was performed using the kits listed in Table S2 according to the manufacturer's instructions.

Cells were acquired at a FACSCantoII flow cytometer (BD Biosciences). If not indicated otherwise, numbers in the dot plots indicate the percentages of cells in the respective gates, numbers in the histograms indicate the mean fluorescence intensity (MFI).

Cell-Cycle and Apoptosis Analysis

For cell-cycle analysis, cells were pulsed for 30 min with BrdU (APC BrdU Flow Kit; BD Biosciences) and stained according to instructions given by the manufacturer. Apoptosis was analyzed using Annexin V binding buffer (BD Biosciences) and staining with Annexin V-Alexa Fluor 647 (BioLegend).

Immunoblotting

Equal amounts of denatured protein were separated by SDS-gel electrophoresis on a 10% gel and transferred onto a PVDF membrane. The membrane was blocked for 1 hr with PBS-T (PBS/0.05% Tween; Sigma) containing 5% BSA (Serva) and washed before probing overnight with the primary antibody diluted in blocking solution. Antibodies used for immunoblotting are listed in Table S3.

After washing steps, the membrane was incubated for 1 hr at room temperature (RT) with horseradish peroxidase (HRP)-coupled secondary goat α-rabbit antibodies diluted in PBS-T/1% BSA. Antibody in excess was washed off, and stained proteins were detected with ECL Ultra Solution kit (Lumigen) on a Fusion SL advanced imaging system (Vilber Lourmat).

Immunohistochemistry

For cryosections, spleens were embedded in OCT-compound (Sakura) and frozen at −80°C. 5-μm sections were prepared using a cryo-microtome (Reichert-Jung 2800 Frigocut) with a S35 knife (Feather) and fixed on SuperfrostPLUS slides (Thermo Scientific) by treatment with pure acetone. Prior to staining the sections were rehydrated with PBS + 2% BSA + 0.1% Na-azide and blocked with Fc-Block (α-CD16/32; BD Biosciences). Sections were stained with the antibodies listed in Table S4. The section was mounted with Fluoromount-G (Southern Biotech). Staining was detected using an Axioskop2 fluorescence microscope (Zeiss, Oberkochen, Germany).

Enzyme-Linked Immunoblot Assay

Mature splenic B cells from the indicated genotypes were cultured in the presence of 2.5 μg/mL LPS from *Escherichia coli* (0111:B4; Sigma-Aldrich) for 1.5 days and subjected to retroviral transduction either with pMIG (EV) or pMIG-*Blimp-1*, respectively. The supernatants were collected 5 days after transduction and used for α-IgM and α-dsDNA-IgM-ELISA.

For the α-IgM and α-IgG ELISAs 96-well plates (NUNC, maxisorp) were coated with polyclonal α-mouse IgM or IgG antibody (SouthernBiotech) and blocked with buffer containing 1% BSA. Dilutions of α-mouse IgM/IgG (SouthernBiotech) were used as standard. The concentration of IgM and IgG in the supernatants was determined by detection with alkaline-phosphatase-labeled α-mouse IgM or IgG (Southern Biotech), respectively. P-nitrophenyl-phosphate (Genaxxon) in diethylamine buffer was added and data were acquired at 405 nm using a Multiskan FC ELISA plate reader (Thermo Scientific). To determine the content of autoreactive IgM antibodies, IgM-concentration-adjusted cell culture supernatants were applied to plates coated with calf thymus DNA (Rockland Immunochemicals). The detection and development was performed as described for the α-IgM ELISA.

(E) ELISpot assay for secretion of IgM and IgG, respectively. IgM$^{-/lo}$/IgD$^-$ splenic B cells derived from mice of the indicated genotypes were FACS-purified and their capacity to secrete antibody was analyzed in triplicate after 16–24 hr of incubation (top). Numbers of dots in the triplicates were quantified (bottom), mean ± SD.
(F) IgM levels measured in sera from *Pten*$^{f/f}$ × CD19-cre × *Bcl2*^{tg} (n = 9), *Pten*$^{f/f}$ × *Bcl2*^{tg} (n = 7), *Pten*$^{f/f}$ × CD19-cre (n = 5), and control mice (n = 3) (mean ± SD).
(G) Splenocytes from *Pten*$^{f/f}$ × CD19-cre, *Pten*$^{f/f}$ × *Bcl2*^{tg}, and *Pten*$^{f/f}$ × CD19-cre × *Bcl2*^{tg} mice were analyzed by flow cytometry for surface expression of CD138 and B220 in the BCR$^+$ (CD19$^+$/B220$^+$/IgM$^+$/IgD$^+$) and BCR$^{-/lo}$ (CD19$^+$/B220$^+$/IgM$^{-/lo}$/IgD$^-$) population of B cells.
See also Figure S7.

ELISpot Assay

$CD19^+/B220^+/IgM^{-/lo}/IgD^-$ were FACS-purified from the spleens of $Pten^{f/f}$ × CD19-cre × $Bcl2^{tg}$ or $Pten^{f/f}$ × $Bcl2^{tg}$ mice, respectively. 5–10 × 10^4 cells per well were plated in triplicates. The assay was performed for IgM and IgG (Mabtech ELISpot Basic [ALP]) according to the manufacturer's instructions.

Quantitative RT-PCR

Cells were purified using a FACSAria IIu sorter (BD Biosciences). RNA was extracted from FACS-sorted cells by using the ReliaPrep RNA Cell Miniprep System (Promega) and cDNA synthesis was performed with the RevertAid Reverse Transcriptase kit (Thermo Fisher) as indicated by the manufacturer. qPCR analysis was performed in triplicate using TaqMan-Probe mixes (Applied Biosystems; listed in Table S5) with TaqMan gene expression mastermix (Applied Biosystems). qRT-PCR data were acquired on a StepOnePlus Real-Time thermocycler (Applied Biosystems) and analyzed with the StepOne Software version 2.3. Results were calculated by applying the ΔΔCT-method.

Statistical Analysis

Graphs were created and statistical analysis was performed using GraphPad Prism (version 6.0h) software. The numbers of individual replicates or mice (n) is stated in the figure legends or the figure itself. If not indicated otherwise p values were calculated by applying two-tailed unpaired t tests. p values < 0.05 were considered to be statistically significant (n. s., not significant; $*p \leq 0.05$; $**p \leq 0.01$; $***p \leq 0.001$; $****p < 0.0001$).

SUPPLEMENTAL INFORMATION

Supplemental Information includes Supplemental Experimental Procedures, seven figures, and seven tables and can be found with this article online at https://doi.org/10.1016/j.celrep.2018.06.035.

ACKNOWLEDGMENTS

We thank Nicole Gust for genotyping, performing ELISA assays, and immunoblotting; Annette Tietz and Johanna Jakob for their contribution in genotyping and analysis of the mice; and Alpaslan Tasdogan and Gabriele Allies for their help with FACS-sorting. We thank Thomas Mertens and Jens von Einem for providing access to the fluorescence microscope.

This work was supported by the DFG through TRR130 (B cells and beyond) project P01, SFB1074, and SFB1279, and ERC advanced grant 694992. H.A. was supported by a PhD scholarship funded by the Egyptian Ministry of Higher Education (MoHE) and the German Academic Exchange Service (DAAD) within the 6th call (2014-2015) of the German-Egyptian Research Long Term Scholarship Program (GERLS; section 441, 91528030; grant number 57030312).

AUTHOR CONTRIBUTIONS

C.S.S. performed experiments, analyzed data, prepared the figures and contributed to writing of the manuscript. E.H., A.K., H.A., M.B., and E.H. performed experiments and analyzed data. H.J. designed the study, supervised the work, and wrote the manuscript.

DECLARATION OF INTERESTS

The authors declare no competing interests.

Received: January 31, 2018
Revised: May 7, 2018
Accepted: June 8, 2018
Published: July 10, 2018

REFERENCES

Alkhatib, A., Werner, M., Hug, E., Herzog, S., Eschbach, C., Faraidun, H., Köhler, F., Wossning, T., and Jumaa, H. (2012). FoxO1 induces Ikaros splicing to promote immunoglobulin gene recombination. J. Exp. Med. *209*, 395–406.

Anderson, K.E., Coadwell, J., Stephens, L.R., and Hawkins, P.T. (1998). Translocation of PDK-1 to the plasma membrane is important in allowing PDK-1 to activate protein kinase B. Curr. Biol. *8*, 684–691.

Bagger, F.O., Sasivarevic, D., Sohi, S.H., Laursen, L.G., Pundhir, S., Sønderby, C.K., Winther, O., Rapin, N., and Porse, B.T. (2016). BloodSpot: a database of gene expression profiles and transcriptional programs for healthy and malignant haematopoiesis. Nucleic Acids Res. *44* (*D1*), D917–D924.

Calado, D.P., Zhang, B., Srinivasan, L., Sasaki, Y., Seagal, J., Unitt, C., Rodig, S., Kutok, J., Tarakhovsky, A., Schmidt-Supprian, M., and Rajewsky, K. (2010). Constitutive canonical NF-κB activation cooperates with disruption of BLIMP1 in the pathogenesis of activated B cell-like diffuse large cell lymphoma. Cancer Cell *18*, 580–589.

Casola, S., Otipoby, K.L., Alimzhanov, M., Humme, S., Uyttersprot, N., Kutok, J.L., Carroll, M.C., and Rajewsky, K. (2004). B cell receptor signal strength determines B cell fate. Nat. Immunol. *5*, 317–327.

Chang, J.E., and Kahl, B.S. (2014). PI3-kinase inhibitors in chronic lymphocytic leukemia. Curr. Hematol. Malig. Rep. *9*, 33–43.

Chiorazzi, N., Rai, K.R., and Ferrarini, M. (2005). Chronic lymphocytic leukemia. N. Engl. J. Med. *352*, 804–815.

Deane, J.A., and Fruman, D.A. (2004). Phosphoinositide 3-kinase: diverse roles in immune cell activation. Annu. Rev. Immunol. *22*, 563–598.

Depoil, D., Weber, M., Treanor, B., Fleire, S.J., Carrasco, Y.R., Harwood, N.E., and Batista, F.D. (2009). Early events of B cell activation by antigen. Sci. Signal. *2*, pt1.

Harwood, N.E., and Batista, F.D. (2008). New insights into the early molecular events underlying B cell activation. Immunity *28*, 609–619.

Heng, T.S., and Painter, M.W.; Immunological Genome Project Consortium (2008). The Immunological Genome Project: networks of gene expression in immune cells. Nat. Immunol. *9*, 1091–1094.

Hobeika, E., Thiemann, S., Storch, B., Jumaa, H., Nielsen, P.J., Pelanda, R., and Reth, M. (2006). Testing gene function early in the B cell lineage in mb1-cre mice. Proc. Natl. Acad. Sci. USA *103*, 13789–13794.

Hoffmann, A., Kerr, S., Jellusova, J., Zhang, J., Weisel, F., Wellmann, U., Winkler, T.H., Kneitz, B., Crocker, P.R., and Nitschke, L. (2007). Siglec-G is a B1 cell-inhibitory receptor that controls expansion and calcium signaling of the B1 cell population. Nat. Immunol. *8*, 695–704.

Hug, E., Hobeika, E., Reth, M., and Jumaa, H. (2014). Inducible expression of hyperactive Syk in B cells activates Blimp-1-dependent terminal differentiation. Oncogene *33*, 3730–3741.

Jellusova, J., Düber, S., Gückel, E., Binder, C.J., Weiss, S., Voll, R., and Nitschke, L. (2010). Siglec-G regulates B1 cell survival and selection. J. Immunol. *185*, 3277–3284.

Johnson, K., Hashimshony, T., Sawai, C.M., Pongubala, J.M., Skok, J.A., Aifantis, I., and Singh, H. (2008). Regulation of immunoglobulin light-chain recombination by the transcription factor IRF-4 and the attenuation of interleukin-7 signaling. Immunity *28*, 335–345.

Klein, U., Casola, S., Cattoretti, G., Shen, Q., Lia, M., Mo, T., Ludwig, T., Rajewsky, K., and Dalla-Favera, R. (2006). Transcription factor IRF4 controls plasma cell differentiation and class-switch recombination. Nat. Immunol. *7*, 773–782.

Knödel, M., Kuss, A.W., Lindemann, D., Berberich, I., and Schimpl, A. (1999). Reversal of Blimp-1-mediated apoptosis by A1, a member of the Bcl-2 family. Eur. J. Immunol. *29*, 2988–2998.

Köhler, F., Hug, E., Eschbach, C., Meixlsperger, S., Hobeika, E., Kofer, J., Wardemann, H., and Jumaa, H. (2008). Autoreactive B cell receptors mimic autonomous pre-B cell receptor signaling and induce proliferation of early B cells. Immunity *29*, 912–921.

Lenz, G., and Staudt, L.M. (2010). Aggressive lymphomas. N. Engl. J. Med. *362*, 1417–1429.

Leslie, N.R., and Downes, C.P. (2002). PTEN: the down side of PI 3-kinase signalling. Cell. Signal. *14*, 285–295.

Maehama, T., and Dixon, J.E. (1998). The tumor suppressor, PTEN/MMAC1, dephosphorylates the lipid second messenger, phosphatidylinositol 3,4,5-trisphosphate. J. Biol. Chem. *273*, 13375–13378.

Mandelbaum, J., Bhagat, G., Tang, H., Mo, T., Brahmachary, M., Shen, Q., Chadburn, A., Rajewsky, K., Tarakhovsky, A., Pasqualucci, L., and Dalla-Favera, R. (2010). BLIMP1 is a tumor suppressor gene frequently disrupted in activated B cell-like diffuse large B cell lymphoma. Cancer Cell *18*, 568–579.

Meixlsperger, S., Köhler, F., Wossning, T., Reppel, M., Müschen, M., and Jumaa, H. (2007). Conventional light chains inhibit the autonomous signaling capacity of the B cell receptor. Immunity *26*, 323–333.

Mercolino, T.J., Arnold, L.W., Hawkins, L.A., and Haughton, G. (1988). Normal mouse peritoneum contains a large population of Ly-1+ (CD5) B cells that recognize phosphatidyl choline. Relationship to cells that secrete hemolytic antibody specific for autologous erythrocytes. J. Exp. Med. *168*, 687–698.

Miletic, A.V., Anzelon-Mills, A.N., Mills, D.M., Omori, S.A., Pedersen, I.M., Shin, D.M., Ravetch, J.V., Bolland, S., Morse, H.C., 3rd, and Rickert, R.C. (2010). Coordinate suppression of B cell lymphoma by PTEN and SHIP phosphatases. J. Exp. Med. *207*, 2407–2420.

Muljo, S.A., and Schlissel, M.S. (2003). A small molecule Abl kinase inhibitor induces differentiation of Abelson virus-transformed pre-B cell lines. Nat. Immunol. *4*, 31–37.

Nguyen, T.T., and Baumgarth, N. (2016). Natural IgM and the development of B cell-mediated autoimmune diseases. Crit. Rev. Immunol. *36*, 163–177.

Nguyen, T.T., Kläsener, K., Zürn, C., Castillo, P.A., Brust-Mascher, I., Imai, D.M., Bevins, C.L., Reardon, C., Reth, M., and Baumgarth, N. (2017). The IgM receptor FcμR limits tonic BCR signaling by regulating expression of the IgM BCR. Nat. Immunol. *18*, 321–333.

Omori, S.A., Cato, M.H., Anzelon-Mills, A., Puri, K.D., Shapiro-Shelef, M., Calame, K., and Rickert, R.C. (2006). Regulation of class-switch recombination and plasma cell differentiation by phosphatidylinositol 3-kinase signaling. Immunity *25*, 545–557.

Painter, M.W., Davis, S., Hardy, R.R., Mathis, D., and Benoist, C.; Immunological Genome Project Consortium (2011). Transcriptomes of the B and T lineages compared by multiplatform microarray profiling. J. Immunol. *186*, 3047–3057.

Piatelli, M., Tanguay, D., Rothstein, T., and Chiles, T. (2003). Cell cycle control mechanisms in B-1 and B-2 lymphoid subsets. Immunol. Res. *27*, 31–52.

Rickert, R.C., Roes, J., and Rajewsky, K. (1997). B lymphocyte-specific, Cre-mediated mutagenesis in mice. Nucleic Acids Res. *25*, 1317–1318.

Savage, H.P., Yenson, V.M., Sawhney, S.S., Mousseau, B.J., Lund, F.E., and Baumgarth, N. (2017). Blimp-1-dependent and -independent natural antibody production by B-1 and B-1-derived plasma cells. J. Exp. Med. *214*, 2777–2794.

Sciammas, R., Shaffer, A.L., Schatz, J.H., Zhao, H., Staudt, L.M., and Singh, H. (2006). Graded expression of interferon regulatory factor-4 coordinates isotype switching with plasma cell differentiation. Immunity *25*, 225–236.

Seifert, M., Sellmann, L., Bloehdorn, J., Wein, F., Stilgenbauer, S., Dürig, J., and Küppers, R. (2012). Cellular origin and pathophysiology of chronic lymphocytic leukemia. J. Exp. Med. *209*, 2183–2198.

Shaffer, A.L., Lin, K.I., Kuo, T.C., Yu, X., Hurt, E.M., Rosenwald, A., Giltnane, J.M., Yang, L., Zhao, H., Calame, K., and Staudt, L.M. (2002). Blimp-1 orchestrates plasma cell differentiation by extinguishing the mature B cell gene expression program. Immunity *17*, 51–62.

Shapiro-Shelef, M., Lin, K.I., McHeyzer-Williams, L.J., Liao, J., McHeyzer-Williams, M.G., and Calame, K. (2003). Blimp-1 is required for the formation of immunoglobulin secreting plasma cells and pre-plasma memory B cells. Immunity *19*, 607–620.

Shapiro-Shelef, M., Lin, K.I., Savitsky, D., Liao, J., and Calame, K. (2005). Blimp-1 is required for maintenance of long-lived plasma cells in the bone marrow. J. Exp. Med. *202*, 1471–1476.

Spaargaren, M., de Rooij, M.F., Kater, A.P., and Eldering, E. (2015). BTK inhibitors in chronic lymphocytic leukemia: a glimpse to the future. Oncogene *34*, 2426–2436.

Srinivasan, L., Sasaki, Y., Calado, D.P., Zhang, B., Paik, J.H., DePinho, R.A., Kutok, J.L., Kearney, J.F., Otipoby, K.L., and Rajewsky, K. (2009). PI3 kinase signals BCR-dependent mature B cell survival. Cell *139*, 573–586.

Stevenson, F.K., and Caligaris-Cappio, F. (2004). Chronic lymphocytic leukemia: revelations from the B-cell receptor. Blood *103*, 4389–4395.

Storch, B., Meixlsperger, S., and Jumaa, H. (2007). The Ig-alpha ITAM is required for efficient differentiation but not proliferation of pre-B cells. Eur. J. Immunol. *37*, 252–260.

Strasser, A., Whittingham, S., Vaux, D.L., Bath, M.L., Adams, J.M., Cory, S., and Harris, A.W. (1991). Enforced BCL2 expression in B-lymphoid cells prolongs antibody responses and elicits autoimmune disease. Proc. Natl. Acad. Sci. USA *88*, 8661–8665.

Suzuki, A., Kaisho, T., Ohishi, M., Tsukio-Yamaguchi, M., Tsubata, T., Koni, P.A., Sasaki, T., Mak, T.W., and Nakano, T. (2003). Critical roles of Pten in B cell homeostasis and immunoglobulin class switch recombination. J. Exp. Med. *197*, 657–667.

Tellier, J., Shi, W., Minnich, M., Liao, Y., Crawford, S., Smyth, G.K., Kallies, A., Busslinger, M., and Nutt, S.L. (2016). Blimp-1 controls plasma cell function through the regulation of immunoglobulin secretion and the unfolded protein response. Nat. Immunol. *17*, 323–330.

Tsiantoulas, D., Gruber, S., and Binder, C.J. (2013). B-1 cell immunoglobulin directed against oxidation-specific epitopes. Front. Immunol. *3*, 415.

Cell Reports, Volume *24*

Supplemental Information

PI3K-Mediated Blimp-1 Activation Controls B Cell Selection and Homeostasis

Corinna S. Setz, Eva Hug, Ahmad Khadour, Hend Abdelrasoul, Mayas Bilal, Elias Hobeika, and Hassan Jumaa

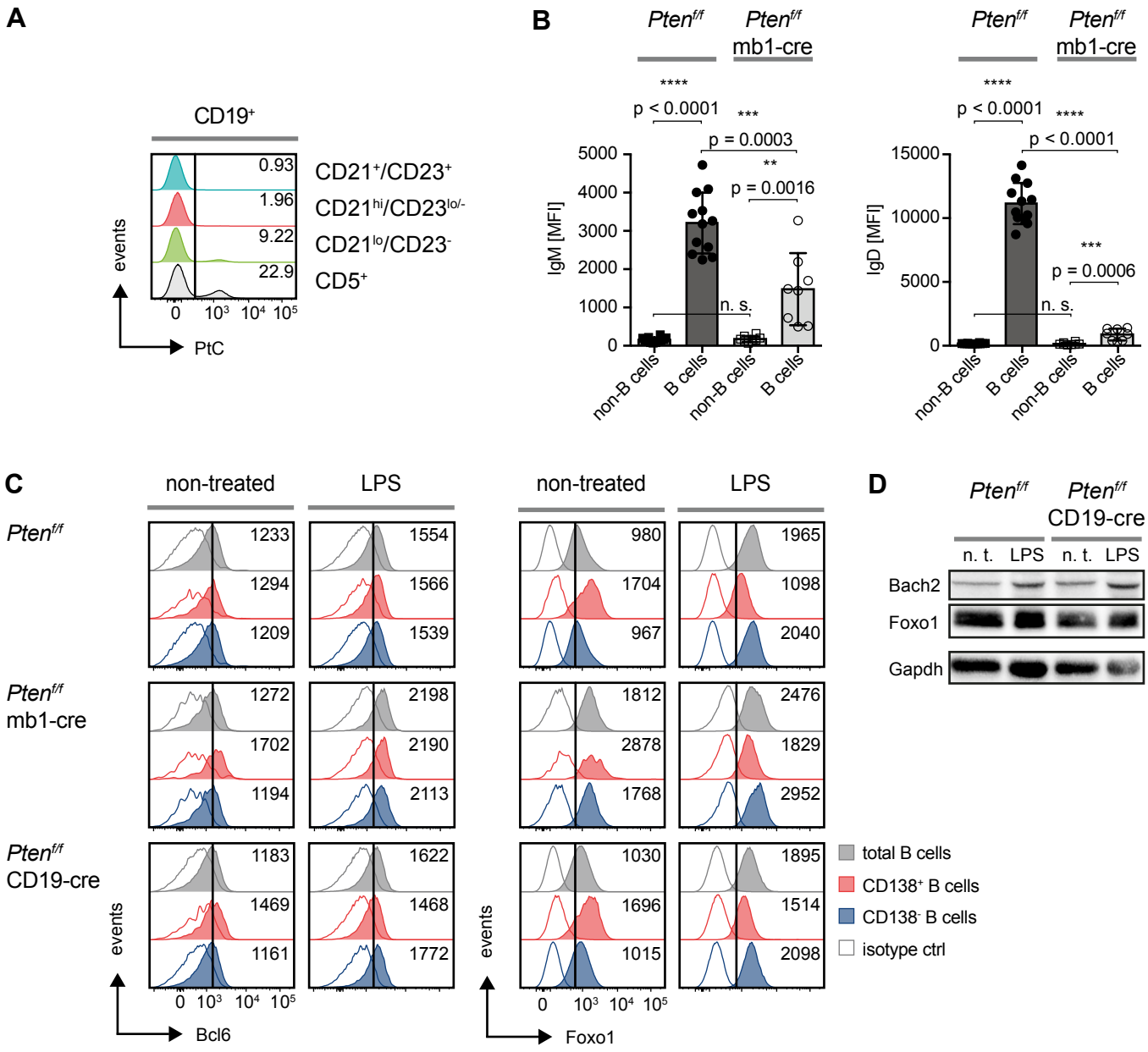

Figure S1 | Reduced BCR Expression in Pten-Deficient Mice and Analysis of Transcription Factors (related to Fig. 1 and 2)

A | Representative flow cytometric analysis of phosphatidylcholine (PtC)-binding in subpopulations of splenic B cells in control mice: Follicular B cells (Fo.B, CD21^{+}/CD23^{+}), marginal zone (MZ.B, CD21^{hi}/CD23$^{lo/-}$) and CD21^{lo}/CD23^{-} B cells.

B | Quantification of IgM (left) and IgD (right) mean fluorescence intensity (MFI) in splenic fractions of B cells and non-B cells from *Pten$^{f/f}$* (n=12) and *Pten$^{f/f}$* x mb1-cre mice (n=8) (mean ±SD). Average MFIs from 3 individual stainings per mouse were calculated. Statistical significance was calculated between B cells and non-B cells from the same mice by using the two-tailed paired t test, otherwise, by applying the two-tailed unpaired t test.

C | Intracellular flow cytometric analysis of Bcl6 (left) and Foxo1 (right) expression in splenocytes from Fig. 2A at day 3 following stimulation with 2.5 µg/ml LPS.

D | Immunoblot analysis of Bach2 and Foxo1 expression in splenocytes from Fig. 2A at day 3. n. t. = non-treated, Gapdh served as loading control. Data are representative of at least 2 mice per genotype.

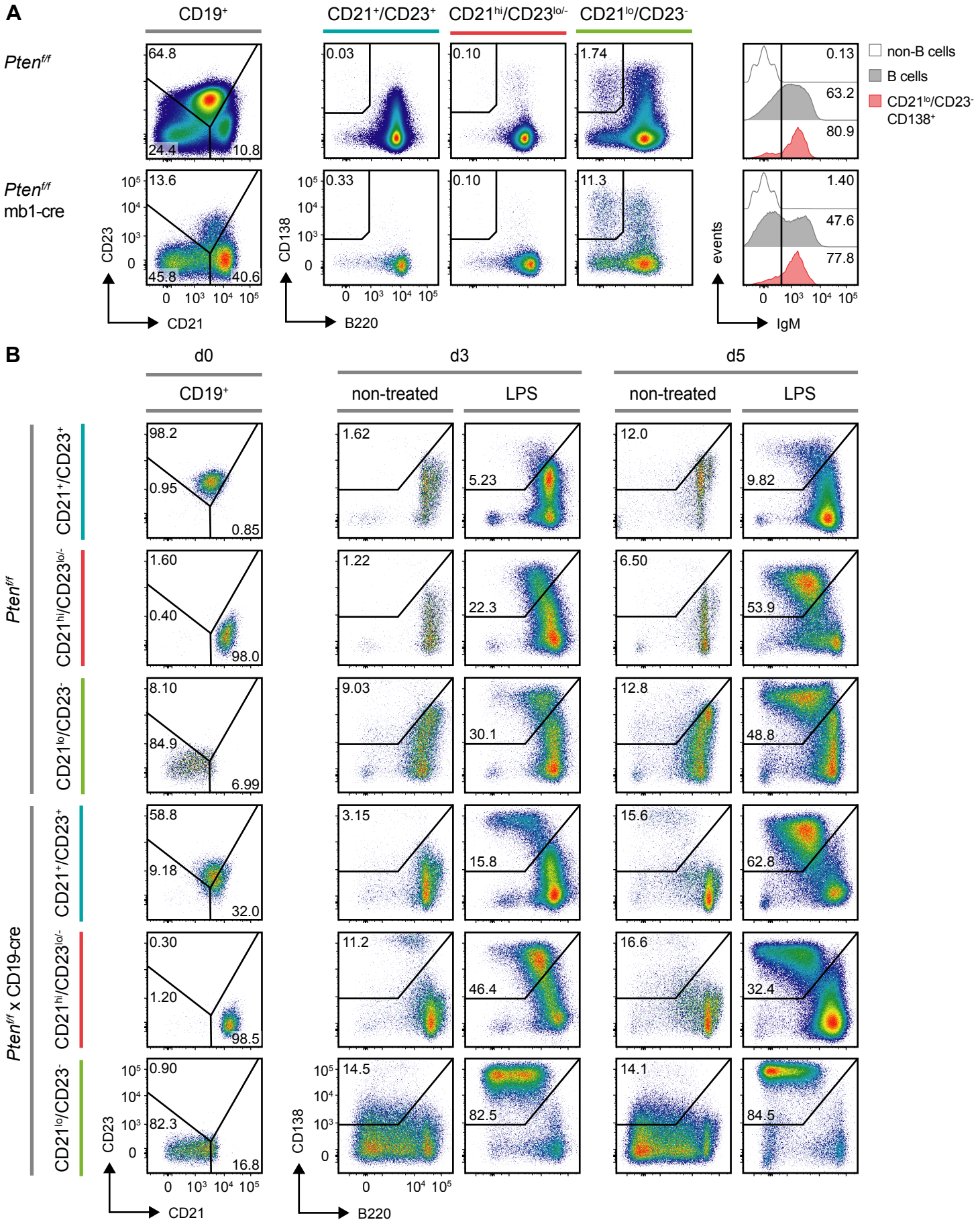

Figure S2 | B Cells From Pten-Deficient Mice are Committed to Terminal Differentiation (related to Fig. 2)

A | Representative staining of CD19^{+}/B220^{lo}/CD138^{+} plasma cells in Fo.B (CD21^{+}/CD23^{+}), MZ.B (CD21^{hi}/CD23$^{lo/-}$) and CD21^{lo}/CD23^{-} splenic B cell subpopulations from *Pten*$^{f/f}$ and *Pten*$^{f/f}$ x mb1-cre mice. CD19^{+}/B220^{lo}/CD138^{+} cells in CD21^{lo}/CD23^{-} B cells were further analyzed for surface IgM expression. Data are representative of at minimum 2 mice per genotype.

B | Fo.B (CD21^{+}/CD23^{+}), MZ.B (CD21^{hi}/CD23$^{lo/-}$) and CD21^{lo}/CD23^{-} splenic B cell populations were FACS-purified from spleens of *Pten*$^{f/f}$ and *Pten*$^{f/f}$ x CD19-cre mice. Cells were either left untreated or cultured in presence of LPS (2.5 µg/ml) for 5 days and surface expression of CD138 and B220 was assessed at the indicated time points. Data are representative of at least 3 mice per genotype.

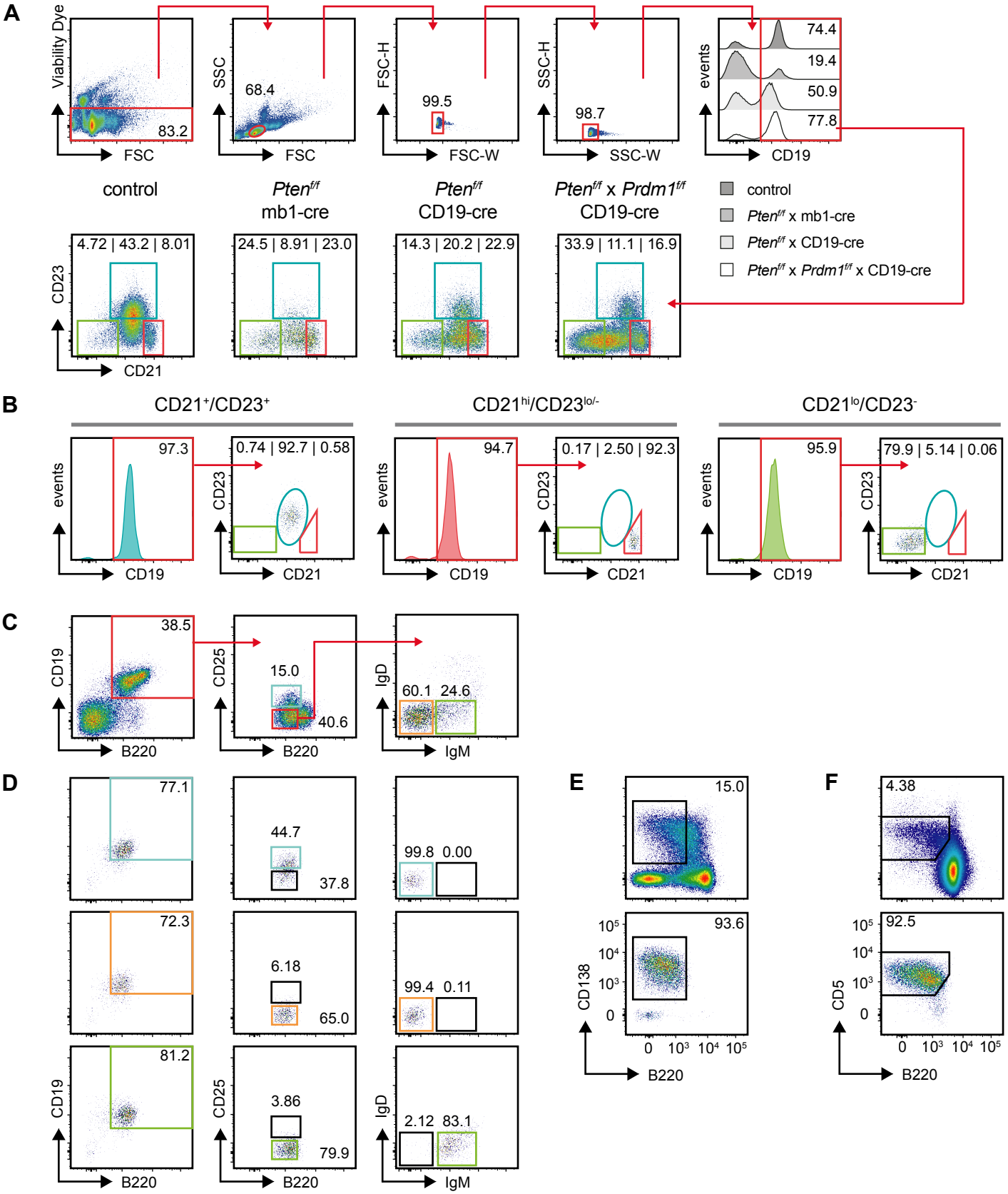

Figure S3 | Increased Blimp-1 Expression in Pten-Deficient B Cells (related to Fig. 2 and 4)

A | Fo.B ($CD21^+/CD23^+$, blue), MZ.B ($CD21^{hi}/CD23^{lo/-}$, red) and $CD21^{lo}/CD23^-$ B cells (green), from spleens of control, *Pten*$^{f/f}$ x mb1-cre, *Pten*$^{f/f}$ x CD19-cre and *Pten*$^{f/f}$ x *Prdm1*$^{f/f}$ x CD19-cre mice were FACS-purified as illustrated by the gating strategy.

B | Representative re-analysis of splenic B cell populations from the control mouse, purified according to the gating strategy shown in Fig. S3A to determine the purity of the sorted populations.

C | Pro-B cells ($CD19^+/B220^+/IgM^-/IgD^-/CD25^-$, orange), small pre-B cells ($CD19^+/B220^+/IgM^-/IgD^-/CD25^+$, blue) and immature B cells ($CD19^+/B220^+/IgM^+/IgD^-/CD25^-$, green) from control mice were FACS-purified as illustrated by the gating strategy.

D | Representative re-analysis of B cell populations purified according to the gating strategy shown in Fig. S3C to determine the purity of the sorted populations.

E | Splenocytes from wild-type mice were stimulated with 2.5 μg/ml LPS for 5 days. $B220^{lo}/CD138^+$ were FACS-purified (top) and subsequently re-analyzed to assess the purity (bottom).

F | Splenic B-1a B cells from wild-type mice (pre-gated on $CD19^+$ cells) were FACS-purified (top) and re-analyzed subsequently to assess the purity (bottom).

Dead cells and doublets were removed also during purification of populations in Fig. S3C, E and F as shown in Fig. S3A.

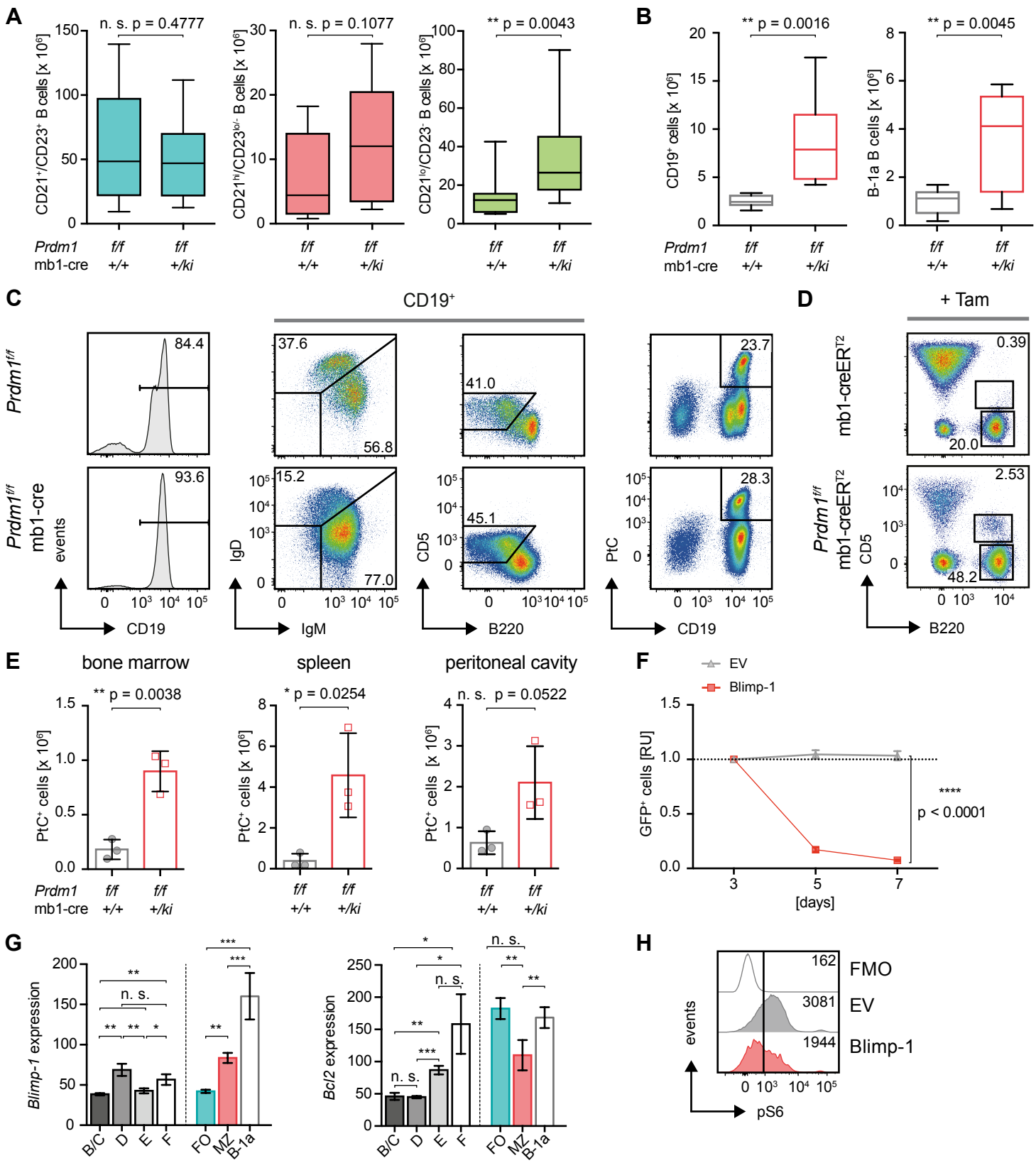

Figure S4 | Increased Autoreactivity in *Prdm1*-Deficient B Cells (related to Fig. 3 and 4)

A | Cell numbers of splenic Fo.B (blue), MZ.B (red) and CD21^{lo}/CD23^{-} (green) B cells from *Prdm1$^{f/f}$* and *Prdm1$^{f/f}$* x mb1-cre mice (n=14, median ±quartile and range).

B | Absolute numbers of total B cells and B-1a B cells in peritoneal cavities from *Prdm1$^{f/f}$* and *Prdm1$^{f/f}$* x mb1-cre mice (n=8, median ±quartile and range).

C | Representative flow cytometric analyses of peritoneal cavity lavages from *Prdm1$^{f/f}$* and *Prdm1$^{f/f}$* x mb1-cre mice for surface expression of the indicated markers and binding of phosphatidylcholine (PtC).

D | Representative flow cytometric analysis of peripheral blood cells from mice of the indicated genotypes 6 months after inducible deletion of *Prdm1* by tamoxifen (+ Tam) administration (bottom). Mice expressing mb1-cre-ER^{T2} in absence of floxed alleles (top) treated with tamoxifen served as control. Shown data are representative for at least 2 individual mice per genotype.

E | Numbers of PtC-reactive B cells in bone marrow, spleens and peritoneal cavities from mice of the indicated genotypes (n=3, mean ±SD).

F | Survival of *Rag2/λ5* double knock-out (DKO) pro-B cells upon ectopic overexpression of Blimp-1 or the empty vector (EV). Percentages of viable GFP^{+} cells at days 5 and 7 were normalized to the percentages measured at day 3 after transduction (n=6, mean ±SD).

G | Analysis of published microarray data on gene expression of *Blimp-1* (left) and *Bcl2* (right) in Hardy fractions B/C (pro), D (pre), E (newly formed) and F (recirculating B cells) compared to expression in Fo.B, MZ.B and B1-a B cells of the murine spleen (n=3 ±SD).

H | Measurement of mTor activity by pS6 content via FACS in *Rag2/λ5* DKO pro-B cells at day 3 upon retroviral transduction with an expression vector encoding Blimp-1 or the EV, respectively. Untransduced cells unstained for pS6 (FMO, fluorescence minus one) served as control.

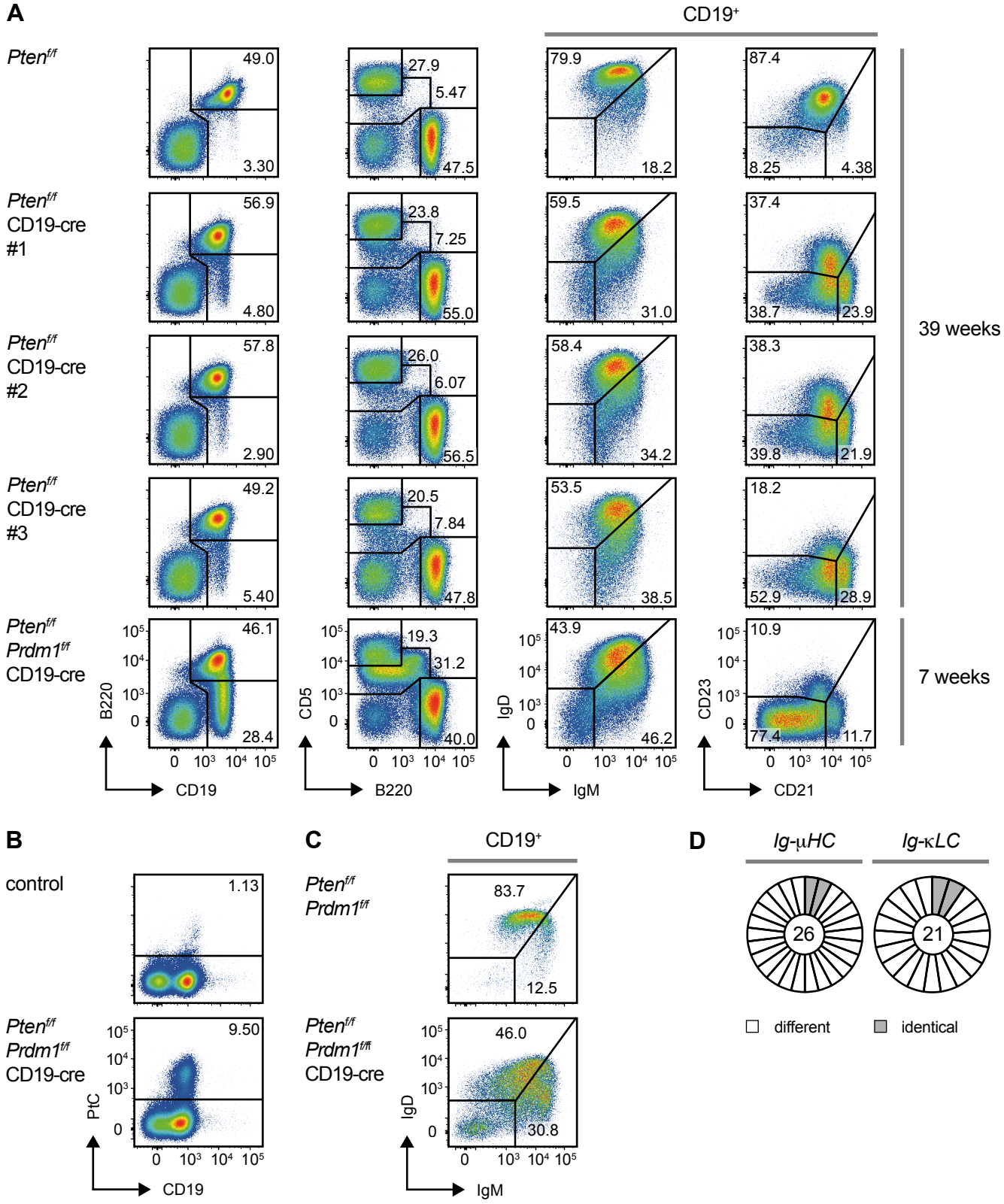

Figure S5 | Premature Terminal Differentiation Prevents Uncontrolled Proliferation (related to Fig. 5)

A | Splenic B cell subpopulations from *Pten*$^{f/f}$, *Pten*$^{f/f}$ x CD19-cre (both sacrificed at the age of 39 weeks) and *Pten*$^{f/f}$ x *Prdm1*$^{f/f}$ x CD19-cre (7 weeks) were compared by flow cytometry.

B | Splenocytes from control and *Pten*$^{f/f}$ x *Prdm1*$^{f/f}$ x CD19-cre mice were analyzed by flow cytometry for surface expression of CD19 and reactivity to phosphatidylcholine (PtC).

C | Peripheral blood from *Pten*$^{f/f}$ x *Prdm1*$^{f/f}$ and *Pten*$^{f/f}$ x *Prdm1*$^{f/f}$ x CD19-cre mice was analyzed by flow cytometry for BCR expression (IgM/IgD).

D | Analysis of V(D)J gene segment usage in CD19^{+}/CD5^{+} B cells from *Pten*$^{f/f}$ x *Prdm1*$^{f/f}$ x CD19-cre mice (n=2). The V(D)J segments from *Ig*-μ*HC* and *Ig*-κ*LC* were cloned from cDNA, sequenced and the frequency of identical combinations was analyzed to assess the BCR clonality of the respective cells in these mice. For further details see also Table S7.

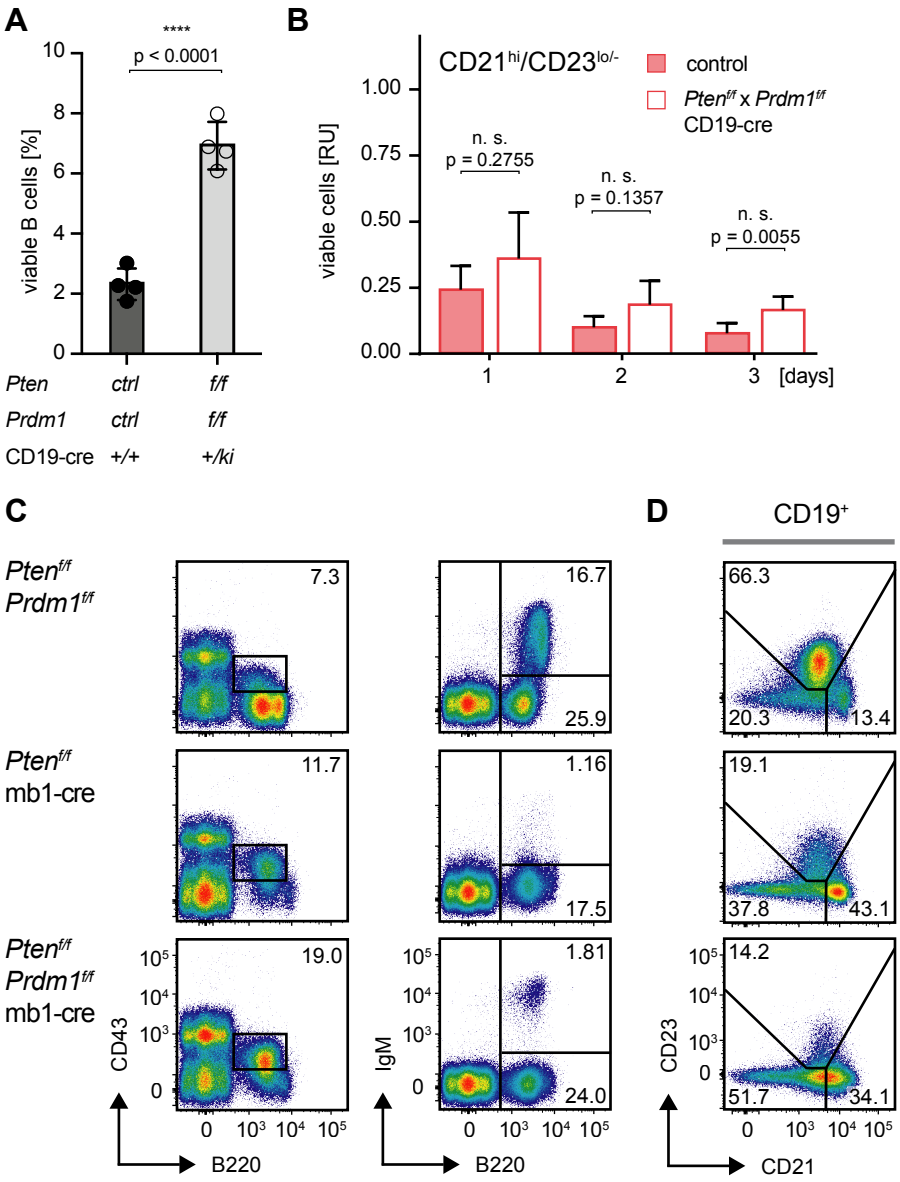

Figure S6 | Reconstitution of Blimp-1 Activates Terminal Differentiation
(related to Fig. 6)

A | Splenocytes from control and *Pten*$^{f/f}$ x *Prdm1*$^{f/f}$ x CD19-cre mice were treated with 2.5 µg/ml LPS. The percentages of viable cells were assessed at 7 days post stimulation by morphology and staining with viability dye, α-CD19 and α-B220 (n=4, mean ±SD).

B | MZ.B cells (CD21^{hi}/CD23$^{lo/-}$) from mice of the indicated genotypes were FACS-purified and cultured *in vitro*. The percentages of viable cells were monitored over a time period of 3 days and assessed by morphology and staining with viability dye. Percentages of viable cells at each timepont were normalized to the percentages of viable cells measured at day 0 in the respective sample (n=4, mean, +SD).

C, D | Freshly isolated bone marrow (**C**) and splenocytes (**D**) from *Pten*$^{f/f}$ x *Prdm1*$^{f/f}$ and *Pten*$^{f/f}$ x *Prdm1*$^{f/f}$ x mb1-cre mice were analyzed by flow cytometry for surface expression of the indicated markers. Data are representative of 2 individual mice sacrificed and analyzed at the age of 10 and 17 weeks, respectively.

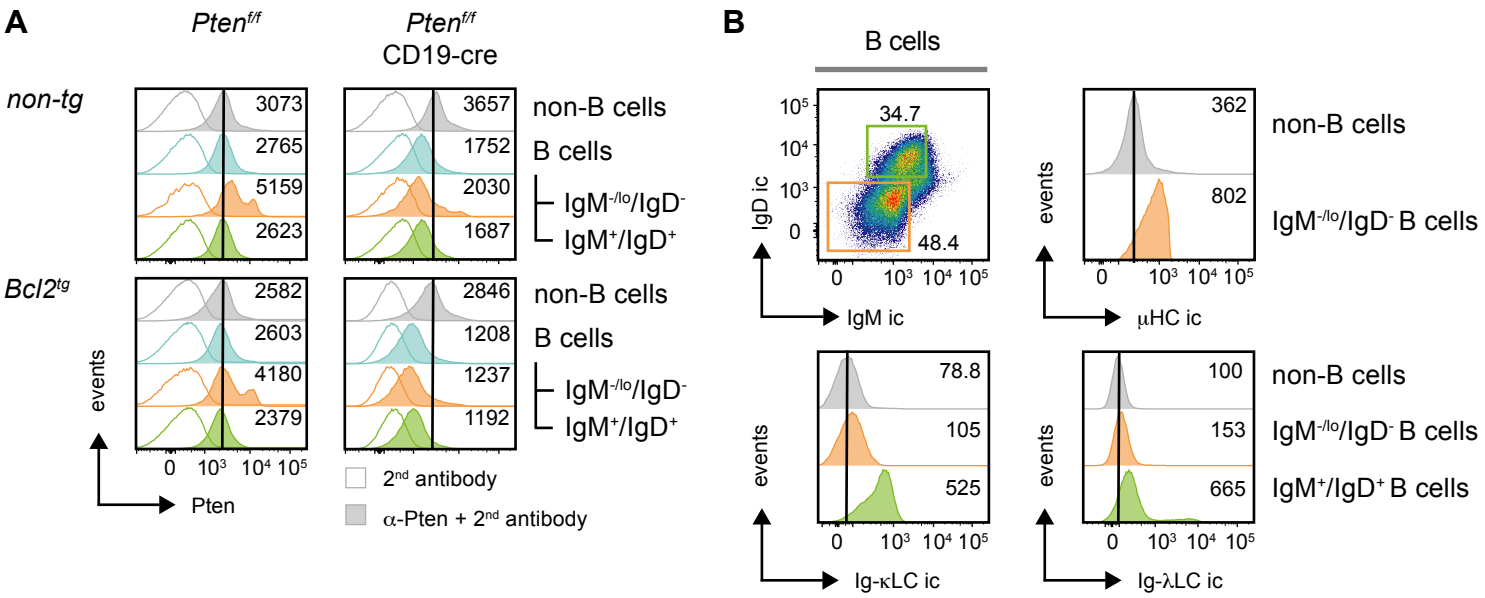

Figure S7 | Characterization of the IgM$^{-/lo}$/IgD^{-} Population in *Pten$^{f/f}$* x CD19-cre x *Bcl2^{tg}* Mice (related to Fig. 7)

A | Splenocytes from mice of the indicated genotypes were stained intracellularly for Pten following surface staining for CD19, B220, IgM and IgD. Pten deletion was compared in the populations of non-B cells (CD19^{-}/B220^{-}), total B cells (CD19^{+}/B220^{+}), BCR^{+} (CD19^{+}/B220^{+}/IgM^{+}/IgD^{+}) and BCR$^{-/lo}$ (CD19^{+}/B220^{+}/IgM$^{-/lo}$/IgD^{-}) B cells.

B | *Pten$^{f/f}$* x CD19-cre x *Bcl2^{tg}*-derived splenocytes were stained at the surface for expression of CD19 and B220, subsequently fixed, permeabilized and stained intracellularly (ic) for IgM, IgD, Ig-κ- and Ig-λLC. Intracellular Ig-μHC expression in the IgM$^{-/lo}$/IgD^{-} population was compared to expression in the non-B cell fraction (CD19^{-}/B220^{-}). Intracellular Ig-κ- and Ig-λLC expression in the IgM$^{-/lo}$/IgD^{-} population was compared to the expression in the IgM^{+}/IgD^{+} B cell and the non-B cell fraction (CD19^{-}/B220^{-}).

Supplemental Experimental Procedures

Tamoxifen Administration

For inducible deletion of *Prdm1*, *Prdm1*$^{f/f}$ mice were intercrossed with mb1-cre-ER^{T2} mice (Hobeika et al., 2015) and treated by gavage 3x every second day with 6 mg tamoxifen (Ratiopharm) dissolved in 20% ClinOleic (Baxter). Inducible deletion of *Prdm1 in vivo* was performed in compliance with animal research permit #1288 at the regional board of Tübingen, Germany). Mice were sacrificed and analyzed 6 months after induction with tamoxifen.

Table S1 | Antibodies used in flow cytometric analyses (related to Experimental Procedures)

Antigen	Conjugate	Clone	Company
CD5	eFluor 450 or PE	53-7.3	eBioscience
CD19	PerCP-Cy5.5	1D3	BD Biosciences
CD19	eFluor 450 or APC	eBio1D3	eBioscience
CD21/CD35	APC or PE-Cy7	7E9	BioLegend
CD23	PE or Biotin	B3B4	BD Biosciences
CD25	APC	PC61	BD Biosciences
CD43	FITC	S7	BD Biosciences
CD45R (B220)	PE-Cy7 or PerCP-eFluor 710	RA3-642	eBioscience
CD138	PE	DL-101	eBioscience
CD138	Brilliant Violet 421	281-2	BioLegend
IgD	FITC, PE or Biotin	11-26	SouthernBiotech
IgD	APC	11-26	eBioscience
IgM	FITC	polyclonal	SouthernBiotech
IgM	eFluor 450	eB121-15-F9	eBioscience
IgM	Cy5	polyclonal	Jackson Immunoresearch
Bcl2	PE	Bcl-2/100	BD Biosciences

Bcl6	Alexa Fluor 647	K112-91	BD Biosciences
Blimp-1	Alexa Fluor 647	5E7	BioLegend
Irf4	eFluor 660	3E4	eBioscience
pS6	PE or PerCP-eFluor710	cupk43k	eBioscience
Pten	unlabeled	138G6	Cell Signaling
Foxo1	unlabeled	C29H4	Cell Signaling
Isotype ctrl.	Alexa Fluor 647 or PE	MOPC-173 and MOPC-21	BioLegend
Isotype ctrl.	eFluor 660	eB149/10H5	eBioscience

Table S2 | Fixation and permeabilization kits used for intracellular flow cytometry (related to Experimental Procedures)

Antigen	Kit	Company
Bcl2, Foxo1, Pten and BCR	Fix and perm cell permeabilization kit	ADG
Bcl6	Foxp3 Staining Buffer Set	eBioscience
Blimp-1 and Irf4	True-Nuclear Transcription Buffer Staining Set	BioLegend
pS6	Cytofix/Cytoperm Kit	BD Biosciences

Table S3 | Antibodies used for immunoblotting (related to Experimental Procedures)

Antigen	origin	Clone	Company
Blimp-1	rabbit	C14A1	Cell Signaling
Bach2	rabbit	polyclonal	Rockland
Irf4	rabbit		abcam
Irf8	rabbit	D20D8	Cell Signaling
Foxo1	rabbit	C29H4	Cell Signaling
pS6	rabbit	D57.2.2E	Cell Signaling
Gapdh	rabbit	D16H11	Cell Signaling

Table S4 | Antibodies used for immunohistochemistry (related to Experimental Procedures)

Antigen	Conjugate	Clone	Company
CD169	FITC	MOMA-1	AbD serotec
CD90.2	PE	53-2.1	BD Biosciences
IgM	Cy5	polyclonal	Jackson Immunoresearch

Table S5 | TaqMan-Probe mixes used for qPCR analyses

(related to Experimental Procedures)

TaqMan-Probe mixes	
Prdm1	Mm00476128_m1
Bcl2	Mm00477631_m1
Gapdh	Mm99999915_g1

RACE

Total RNA was isolated from sorted cells and cDNA was synthesized as described in the main experimental procedures section concerning quantitative RT-PCR. A poly G-tail was added to the 3' end of the first strand cDNA using dGTP and TdT (New England Biolabs). *Ig-μHC*-specific and *Ig-κLC*-specific transcripts were amplified by nested PCR using gene-specific oligos, anchor/adaptor oligos (enlisted in Table S6) and Q5 polymerase (New England Biolabs). The amplified PCR-products were subcloned in pJET1.2 blunt/vector (CloneJET PCR Cloning Kit, Thermo Fisher) and colonies were sequenced (GATC). Sequences were analyzed by using the ImMunoGeneTics information system IMGT/V-Quest online tool.

Table S6 | Primers used for *Ig* gene RACE (related to Experimental Procedures)

Ig-μHC amplification

Primers 1st PCR		Sequence 5'→ 3'
BaPpc	Anchor	CTC TGC AGG ATC CAC GAC CCC CCC CCC CCC C
mmuSP2		GAC CAG ACA GGT CAG GTT AGC GGA CTT GCT

Primers 2nd PCR		Sequence 5'→ 3'
BaP	Adaptor	TCT GCA GGA TCC ACG ACC
mmuSP3		GAT GAC TTC AGT GTT GTT CTG GTA GTT CCA

Ig-κHC amplification

Primers 1st PCR		Sequence 5'→ 3'
BaPpc	Anchor	CTC TGC AGG ATC CAC GAC CCC CCC CCC CCC C
mK-SP2		TGA AGT TGA TGT CTT GTG AGT GGC CTC

Primers 2nd PCR		Sequence 5'→ 3'
BaP	Adaptor	TCT GCA GGA TCC ACG ACC
mK-SP1		TCA AGA AGC ACA CGA CTG AGG

Table S7 | *Ig* gene RACE sequencing results (related to Fig. 5 and Fig. S5D)

Ig-μHC

# 5462 DKO CD19⁺ CD5⁺					
Clone N.	V-GENE and allele	J-GENE and allele	D-GENE and allele	HCDR3	Length
C 16	IGHV1-12*01 F	IGHJ2*01 F	IGHD2-3*01 F	CARDVHFDYW	8
C 17	IGHV1-59*01 F	IGHJ3*01 F	IGHD2-3*01 F	CAREGDGYAYW	9
C 21	IGHV5-17*01 F	IGHJ4*01 F	IGHD2-14*01 F	CARQYRAMDYW	9
C 22	IGHV5-17*01 F	IGHJ4*01 F	IGHD2-14*01 F	CARPRYHTMDYW	10
C 23	IGHV1-72*01 F	IGHJ2*01 F	IGHD2-10*02 F	CAYGNYVYYFDYW	11
C 24	IGHV1-77*01 F	IGHJ3*01 F	IGHD2-2*01 F	CARGGGYVLFAYW	11
C 25	IGHV11-2*01 F	IGHJ1*03 F	IGHD1-1*01 F	CMRYGSSYWYFDVW	12
C 26	IGHV9-3*01 F	IGHJ3*01 F	IGHD2-3*01 F	CARPDGYLFAYW	10
C 27	IGHV1-75*01 F	IGHJ3*01 F	IGHD3-3*01 F	CARGGTGFAYW	9
C 28	IGHV6-6*01 F	IGHJ2*01 F	IGHD1-1*01 F	CTRHYGSSYYFDYW	12
C 29	IGHV9-4*01 F	IGHJ3*01 F	IGHD1-1*01 F	CARSYYYGSSYSWFAYW	15
C 30	IGHV1-50*01 F	IGHJ2*01 F	IGHD1-1*02 F	CARGDYFDYW	8

# 5464 DKO CD19⁺ CD5⁺					
	V-GENE and allele	J-GENE and allele	D-GENE and allele	HCDR3	Length
C 44	IGHV5-9-1*02 F	IGHJ4*01 F	IGHD2-3*01 F	CTRDDDGYFYYYAMDYW	15
C 45	IGHV8-8*01 F	IGHJ2*01 F	IGHD2-10*01 F	CARTPYYGRGFDYW	12
C 46	IGHV9-3*01 F	IGHJ4*01 F	IGHD2-2*01 F	CARTTTDTAMDYW	11
C 47	IGHV1-19*01 F	IGHJ1*03 F	IGHD2-1*01 F	CARVYGNWYFDVW	11
C 48	IGHV9-3*01 F	IGHJ2*01 F	IGHD3-3*01 F	CARIGGLYYFDYW	11
C 49	IGHV2-9-1*01 F	IGHJ3*01 F	IGHD2-2*01 F	CARYGYDGGPWFAYW	13
C 50	IGHV1-19*01 F	IGHJ3*01 F	IGHD1-1*02 F	CGGGNYGWFAYW	10
C 51	IGHV1-63*01 F	IGHJ3*01 F	IGHD3-1*01 F	CARGLTWFAYW	9
C 52	IGHV5-6*01 F	IGHJ1*03 F	IGHD2-4*01 F	CARPLYDYDYWYFDVW	14
C 53	IGHV1-55*01 F	IGHJ2*01 F	no	CARRDYW	5
C 54	IGHV5-17*01 F	IGHJ1*03 F	IGHD2-3*01 F	CARCYYRYFDVW	10
C 55	IGHV1-19*01 F	IGHJ2*01 F	IGHD2-4*01 F	CARGLDYDGGYW	10
C 56	IGHV11-2*01 F	IGHJ1*03 F	IGHD2-1*01 F	CMRYGNYWYFDVW	11
C 57	IGHV9-3*01 F	IGHJ2*01 F (a)	IGHD6-3*01 F	CARDSTVDYW	8

Ig-κLC

# 5462 DKO CD19⁺ CD5⁺				
Clone N.	V-GENE and allele	J-GENE and allele	LCDR3	Length
C 2	IGKV8-27*01 F	IGKJ5*01 F	CHQYLSSLTF	8
C 10	IGKV3-10*01 F	IGKJ2*01 F	CQQNNEDPYTF	9
C 11	IGKV8-16*01 F	IGKJ2*01 F	CQQHLHIPYTF	9
C 12	IGKV17-121*01 F	IGKJ5*01 F	CLQSDNLPLTF	9
C 14	IGKV14-126*01 F	IGKJ4*01 F	CLQHGESPFTF	9
C 19	IGKV14-126*01 F	IGKJ1*01 F	CLQHGESPWTF	9
C 26	IGKV12-44*01 F	IGKJ2*01 F	CQHHYGTPYTF	9
C 29	IGKV4-91*01 F	IGKJ5*01 F	CQQGSSIPLTF	9
C 31	IGKV8-16*01 F	IGKJ4*01 F	CQQHLHIPYTF	9

# 5464 DKO CD19⁺ CD5⁺				
	V-GENE and allele	J-GENE and allele	LCDR3	Length
C 3	IGKV5-39*01 F	IGKJ5*01 F	CQNGHSFPLTF	9
C 5	IGKV8-24*01 F	IGKJ1*01 F	CQQHYSTPRTF	9
C 6	IGKV4-91*01 F	IGKJ5*01 F	CQQGSSIPLTF	9
C 7	IGKV5-39*01 F	IGKJ4*01 F	CQNGHSFPFTF	9
C 9	IGKV4-59*01 F	IGKJ2*01 F	CQQWSSYPYTF	9
C 12	IGKV5-39*01 F	IGKJ2*01 F	CQNGHSFPYTF	9
C 16	IGKV14-126*01 F	IGKJ2*01 F	CLQHGESPYTF	9
C 19	IGKV12-44*01 F	IGKJ2*01 F	CQHHYGTPYTF	9
C 20	IGKV8-21*01 F	IGKJ1*01 F	CKQSYNLPWTF	9
C 23	IGKV5-39*01 F	IGKJ2*01 F	CQNGHSFPYTF	9
C 25	IGKV8-21*01 F	IGKJ1*01 F	CKQSYNLPWTF	9
C 27	IGKV19-93*01 F	IGKJ1*01 F	CLQYDNLWTF	8

Identical V(D)J segments are marked in grey

Supplemental references

Hobeika, E., Levit-Zerdoun, E., Anastasopoulou, V., Pohlmeyer, R., Altmeier, S., Alsadeq, A., Dobenecker, M.W., Pelanda, R., and Reth, M. (2015). CD19 and BAFF-R can signal to promote B-cell survival in the absence of Syk. EMBO J *34*, 925-939.